Journal of Volcanology and Geothermal Research 282 (2014) 115–133

Contents lists available at ScienceDirect

Journal of Volcanology and Geothermal Research

journal homepage: www.elsevier.com/locate/jvolgeores

# Morphometry of subaerial shield volcanoes and glaciovolcanoes from Reykjanes Peninsula, Iceland: Effects of eruption environment

G.B.M. Pedersen [a,*], P. Grosse [b]

[a] Nordic Volcanological Center, Institute of Earth Sciences, University of Iceland, Sturlugata 7, 101 Reykjavík, Iceland
[b] CONICET(Consejo Nacional de Investigaciones Científicas y Técnicas) and Fundación Miguel Lillo, San Miguel de Tucumán, Argentina

ARTICLE INFO

*Article history:*
Received 31 January 2014
Accepted 2 June 2014
Available online 21 June 2014

*Keywords:*
Morphometry
Intraglacial volcanoes
Tuya
Shield volcanoes
Reykjanes Peninsula
Iceland

ABSTRACT

We present a morphometric study of 33 basaltic volcanic edifices from the Reykjanes Peninsula, Iceland, using a 20 m resolution digital elevation model (DEM). Slope values distinguish subaerial from intraglacial eruption environments, with glaciovolcanic edifices having average slope values that are >5° higher than subaerial shields. The 26 analyzed glaciovolcanic edifices are separated into 3 groups based on size, and are also categorized following the new classification scheme of tuyas by Russell et al. (2014), into 15 tindars, 1 conical tuya, 3 flat-topped tuyas and 7 complex tuyas.

The glaciovolcanic edifices show a continuum of landforms ranging from small elongated tindars to large equidimensional flat-topped tuyas. The smaller edifices (<0.01 $km^3$) are all tindars and the larger edifices (>0.1 $km^3$) are flat-topped tuyas. The mid-sized edifices (0.01–0.1 $km^3$) show a wide variety of shapes and classify either as tindars or as complex tuyas, with only one edifice classifying as a conical tuya. Edifice elongation tends to decrease with volume, suggesting that small edifices are primarily fissure controlled, whereas larger edifices are mainly controlled by a central vent. The mid-sized complex tuyas are transitional edifices, suggesting that some intraglacial eruptions start as fissure eruptions that subsequently concentrate into one or more central vents, whereas the mid-sized tindars suggest a sustained fissure eruption.

There is a tectonic control on the orientation of the edifices evidenced by a strong correlation between edifice elongation azimuth and mapped faults and fractures. Most edifice elongations cluster between 020° and 080°, coinciding with the strike of normal faults within and at the boundary of regional volcanic systems, but some edifices have elongations that correlate with N–S striking book-shelf faults. This implies that intraglacial eruptions are controlled by pre-existing pathways in the crust, as has been previously observed for subaerial fissure eruptions.

In terms of classification, quantification of the limits between the four tuya types proposed by Russell et al. (2014) is difficult because of the transitional nature shown by several edifices. A threshold of 1.8 in ellipticity index (E.I.) values can be used to distinguish tindars from the other three types. Flat-topped tuyas are distinguished by their greater overall size, their large and relatively flat summit regions, reflected in bimodal slope distributions, and their low E.I. and low to intermediate irregularity index (I.I.) values. The only analyzed conical tuya has very low E.I. and I.I. values, very small summit regions and very steep flank slopes. The complex tuyas have variable morphometries, but are in general characterized by high I.I. values and very irregular slope distributions. No correlation is observed between edifice-scale morphology and lithology (e.g. pillow dominated or hyaloclastite dominated).



## 1. Introduction

The geomorphometry of a volcano is an important source of information. Not only is it a record of the interplay between constructional and destructional processes, but it is also essential for the evaluation of future activity and hazard assessment (e.g. Schilling, 1998; Kervyn et al., 2007; Favalli et al., 2009). In addition, geomorphometry has been successfully implemented for advanced mapping techniques in other fields (e.g. van Asselen and Seijmonsbergen, 2006; Romstad and Etzelmuller, 2009) and is likely applicable to volcano mapping as well.

Today, remote sensing-derived digital elevation models (DEM) provide comprehensive topographic data at medium-to-high spatial resolution allowing varied and detailed geomorphometric analysis on a regional to global scale. Despite the plethora of data, investigation of volcano morphometry has been rather limited (as mentioned by Davidson and De Silva, 2000; Francis and Oppenheimer, 2004) and has primarily focused on the morphometry of specific volcanic landforms such as cinder cones (e.g. Porter, 1972; Wood, 1980a; Fornaciai et al., 2012), oceanic basaltic shields (Moore and Mark, 1992; Rowland

* Corresponding author. Tel.: +354 5254496; fax: +354 562 9767.
*E-mail address:* grobirkefeldt@gmail.com (G.B.M. Pedersen).

http://dx.doi.org/10.1016/j.jvolgeores.2014.06.008

and Garbeil, 2000; Robinson and Eakins, 2006) and, less commonly, composite volcanoes (Grosse et al., 2009; Karátson et al., 2010).

Morphometric studies based on DEMs have the advantage of allowing analysis of remote and inaccessible volcanoes, including submarine (e.g. Clague et al., 2011; Caress et al., 2012; Wormald et al., 2012) and extraterrestrial volcanoes (e.g. Pike, 1978; Wood, 1979; Plescia, 2004). However, constraining the topographic characteristics of terrestrial volcanoes is an essential step for use of volcano geomorphometry for comparative planetology.

In this study, we investigate the morphometry of a variety of volcanic landforms on the Reykjanes Peninsula, Iceland, characterizing and classifying them in association with their subaerial or intraglacial eruption environments.

### 1.1. Volcano geomorphometry

Volcanic landforms are the result of constructional and destructional forces. The geomorphometry of a volcano evolves depending on the prevailing processes and therefore contains information on various factors such as eruptive activity and environment, magma composition, stress regime, and erosion, as well as more catastrophic processes related to flank collapse and tectonics (Francis and Oppenheimer, 2004; Grosse et al., 2009).

Extraction of information based on volcano geomorphometry can be very complex and monogenetic volcanoes have received special attention because of their relatively simple morphology and widespread distribution. Overall, studies of monogenetic cones focus on morphometric parameters such as height, basal width and crater width, and have included (1) historical documentation of cone growth (e.g. Wood, 1980a), (2) definition of different types of monogentic cones (e.g. Porter, 1972; Wood, 1980a), (3) correlation between cone morphometry and degradation as a proxy for age (e.g. Wood, 1980b; Inbar et al., 2011), (4) experimental analogs to analyze factors influencing morphometry (e.g. Kervyn et al., 2012), and (5) modeling of emplacement mechanisms and degradation (e.g. Fornaciai et al., 2012; Broz et al., 2013).

Investigations of shield volcano morphometry have mostly relied on the same parameters used for monogenetic cones (e.g. Pike, 1978; Hasenaka, 1994; Rossi, 1996), and morphometry has also been used to estimate volumes and thereby magma output rate (e.g. Hasenaka, 1994; Robinson and Eakins, 2006). In addition, geomorphometric analyses of shield volcanoes have focused on the measurement of edifice slopes. Moore and Mark (1992) investigated slope frequencies and slope development as a function of elevation at Hawaiian shields, showing that they become steeper with age as a result of the change from tholeiitic to more viscous alkali lavas. Similar studies were carried out for the Galapagos shields (Mouginis-Mark et al., 1996; Rowland, 1996), which were divided into two groups based on slope distribution. Rowland and Garbeil (2000) summarized the morphological spectrum of oceanic shields and related constructional and destructional processes to specific slope values.

Composite cones (e.g. stratovolcanoes) have, from a morphometric perspective, received less attention. A few studies (e.g. Pike, 1978; Garvin, 1996; McKnight and Williams, 1997) differentiate between monogenetic and composite cones by comparing morphometric parameters such as height, base width and crater width. More recent studies use DEMs and derived data to reconstruct eroded volcanic landforms (e.g. Székely and Karátson, 2004; Karátson et al., 2010) or to trace the growth evolution of a single (e.g. Michon and Saint-Ange, 2008) or a group of volcanoes (Grosse et al., 2009; Karátson et al., 2010).

Morphometry is a primary data source for investigation of submarine volcanoes. Bathymetric DEMs have been used to delineate and calculate lava volumes (Caress et al., 2012), to map the structures and evolutions of volcanic centers (Wormald et al., 2012), and to correlate effusive and explosive eruptions with depth and volcano morphology (Strech et al., 2006; Clague et al., 2011).

Morphometric data have also proven essential in studies of extraterrestrial volcanoes residing on our Moon, Venus, Mars and Io (Pike, 1978; Wood, 1979; Smith, 1996; Kortz and Head, 2001). The morphometric parameters used in these studies have mainly been edifice height, basal width, crater width and slope (e.g. Pike, 1978; Wood, 1979; Plescia, 2004) and have focused on using the morphometric parameters for classification of volcano type. A few investigations have extended the studies to include predictions on viscosity of lavas and flow rate on Io (Schenk et al., 2004) and Mars (Baratoux et al., 2009).

The variety of studies and applications reflect the importance of volcano geomorphometry. However, they also show that a systematic methodology to extract morphometric information is lacking. Grosse et al. (2012) pointed out that systematic DEM-based analysis on a global scale requires (1) a comprehensive set of morphometric parameters applicable to a variety of volcanic landforms, and (2) an objective and consistent approach to delineate edifice boundaries. Therefore, Grosse et al. (2009, 2012) and Euillades et al. (2013) developed a standardized methodology for edifice delineation as well as a standardized set of morphometric parameters useful for geomorphometric analysis. They used this methodology to evaluate growth stages and morphometric evolution of arc volcanoes in Central America and southern Central Andes (Grosse et al., 2009) and to construct a global database of composite volcano morphometry (Grosse et al., 2014).

### 1.2. Glaciovolcanic edifices

Glaciovolcanic edifices are volcanoes that formed in contact with or confined by ice, resulting in distinct morphology and lithofacies (Russell et al., 2014). A qualitative model of glaciovolcano formation was developed in the 1940s to 1960s based on geological mapping in both Iceland and British Colombia, Canada (e.g. Noe-Nygaard, 1940; Matthews, 1947; Van Bemmelen and Rutten, 1955; Kjartansson, 1966; Jones, 1969). This model divides the formation of glaciovolcanic edifices into different phases producing different lithologies (Fig. 1). The initial phase of subglacial volcanic activity will depend on the ice-thickness at the eruption site. If the ice is sufficiently thick the eruption will start out as an effusive pillow lava-producing eruption, where magmatic heating will melt the ice sheet creating a melt-water vault that confines the pillow lavas, creating a steep-sided lava pile (Fig. 1, phase 1). If the initial ice thickness is thin, or if the eruption continues long enough, the overlying pressure from ice and melt-water is sufficiently low to allow an explosive phase, producing fragmented glassy volcanoclastic deposits with variable clast-sizes such as hyaloclastite and hyalotuff (Fig. 1, phase 2). This deposit will be confined by the englacial lake and will eventually build-up above the lake level, changing the eruption style to a subaerial lava-producing eruption. The lava issuing from the vent will flow into the lake, where it will granulate creating a lapilli tuff/tuff-breccia building out as a delta with inclined foresets equal to the angle of repose, and subsequently capped with upstream lava (Fig. 1, phase 3). The zone of transition between the lapilli tuff/tuff-breccia and the lava cap was defined as the passage zone by Jones (1969). It marks the englacial lake level at the time of the transition to subaerial eruptive activity and may be used as indicator of ice sheet surface elevation at the time of eruption (e.g. Walker, 1965; Jones, 1969; Jones and Nelson, 1970; Smellie, 2000).

Research on glaciovolcanoes has expanded significantly in the last decades, leading to a diversified scientific community using different nomenclature. Russell et al. (2014) provide a comprehensive compilation of published nomenclature of glaciovolcanic landforms. Here, we summarize the most widely-used nomenclature and refer to Russell et al. (2014) for a more extensive review on classification schemes.

Typically, glaciovolcanic edifices have been divided into the following landforms: (1) flat-topped mountains called tuyas (also known as starpar/table mountains), (2) ridges called tindars (also named hryggir/hyaloclastite ridges/moberg ridges), and (3) cone-shaped mountains (e.g. Matthews, 1947; Van Bemmelen and Rutten, 1955; Kjartansson, 1966; Jones, 1969; Allen et al., 1982). A geomorphic distinction between

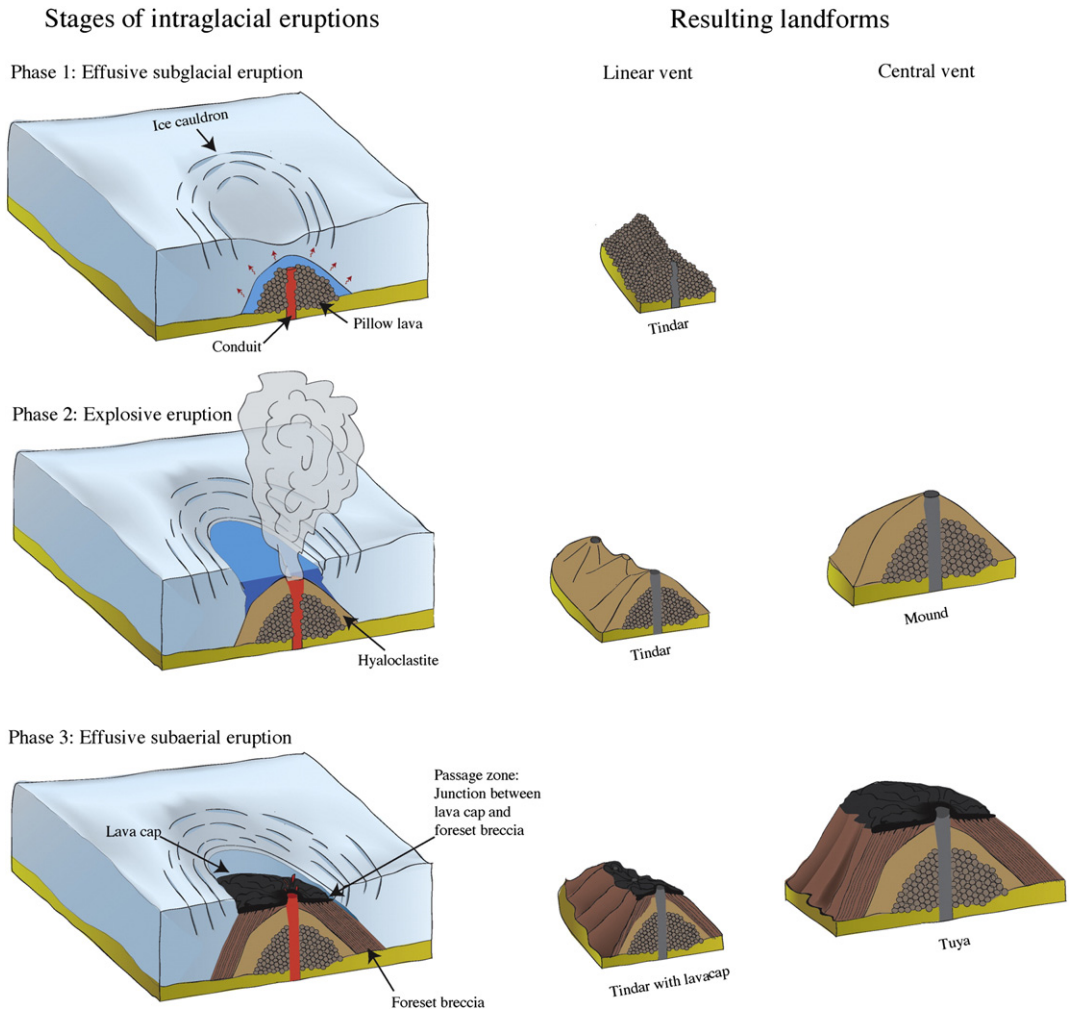


**Fig. 1.** Diagram showing the different stages of intraglacial eruptions and the resulting landforms depending on vent geometry. See text for explanation. Modified after Jones (1969) and Hickson (2000).

tindars and tuyas has been proposed using a 2:1 length to width (L/W) ratio as the division between tuyas and elongated tindars (Hickson, 2000; Jakobsson and Gudmundsson, 2008).

A more extensive classification scheme for glaciovolcanic edifices was developed by Smellie (2007) consisting of 7 different kinds of landforms divided into mafic and felsic types. The variety of landforms was suggested to result from differences in lithofacies, in properties of the enclosing ice and in magma composition, discharge rate and volatile content. This classification scheme was assessed morphometrically using parameters such as volume, area, height, width and length. The analysis showed that the mafic tuyas volumetrically exceed any other type of glaciovolcanic edifice and that the height versus width ratio can be used to separate felsic from mafic glaciovolcanic edifices. Smellie (2007) also proposed a hierarchical relationship between glaciovolcanic landforms suggesting possible evolutionary trends (e.g. a pillow tindar/mound may evolve into a tephra tindar/mound and subsequently into a tuya).

The most recent nomenclature and classification scheme has been presented by Russell et al. (2014), aiming at unifying previous nomenclatures. It contains a definition of "tuya" and a descriptive and genetic classification scheme. Their definition of tuya is "positive-relief volcanoes having a morphology resulting from ice confinement during eruption and comprising a set of lithofacies reflecting direct interaction between magma and ice/melt water." (p. 70, Russell et al., 2014). The subsequent subdivision of tuyas is hierarchical and is first based on (1) edifice-scale morphology (2) proportions of lithofacies, and (3) magma composition. They distinguish four subtypes of tuyas based on morphology, namely (1) flat-topped tuya; (2) conical tuya; (3) linear tuya or tindar (L/W > 2), and (4) Complex tuya. As in previous studies, the only quantitative distinction is that of the length to width ratio to separate the elongated landforms. The additional 'complex tuya' subtype reflects the existence of glaciovolcanoes with substantial variation in eruption style, and/or longer-lived activity. The lithofacies and composition modifiers allow further distinction between edifices and provide further information on primary eruption style and magma chemistry.

Both Smellie (2007) and Russell et al. (2014) note that their classification schemes are based on primary morphologies, ignoring possible post-eruptive erosional effects. Russell et al. (2014) acknowledge that this is a caveat in their classification system since potential post-eruptive modification may create a conical shaped remnant from an originally flat-topped edifice. Potential degradation processes include failure of over-steepened slopes, gully formation, debris flow, and cirque/valley glaciation (Komatsu et al., 2007). The absence of tindars in some parts of the Icelandic neovolcanic zone has been suggested to correlate with fast flowing ice streams and hence, Bourgeois et al. (1998) proposed that glaciovolcanic edifices only survive near ice divides and in areas with slow moving ice. However, other evidence shows that 4.6 Ma lava caps can survive unmodified in a polythermal glacial regime (Smellie et al., 2008). Knowledge of the effects of glacial erosion on glaciovolcanic landforms is sparse and a quantitative assessment of its impact on edifice morphology is lacking.

Furthermore, Smellie (2007) mentions that his classification scheme is biased towards glaciovolcanic edifices produced by short-lived monogenetic eruptions, leaving out long-lived polygenetic edifices. Russell et al. (2014) include these edifices in the "complex tuyas" category, together with seemingly monogenetic edifices that show varied eruption styles. However, they do not address whether the categories of "flat-topped tuya", "conical tuya" and "linear tuya or tindar" are assumed to be monogenetic or polygenetic.

In this article, we adopt the classification scheme of Russell et al. (2014), because of its emphasis on morphology, which is very well suited for our morphometric study. We will thus use the terms "flat-topped tuya", "conical tuya", "complex tuya" and "tindar" (for linear tuyas).

## 2. Study area

The Reykjanes Peninsula, SW Iceland (Fig. 2), was chosen as the study area because it hosts a variety of well preserved subaerial and intragalcial volcanic edifices. Moreover, the peninsula is among the youngest and most pristine parts of Iceland and has recently been completely mapped at 1:100,000 scale by Saemundsson et al. (2010).

The Reykjanes Peninsula is the direct onshore continuation of the Mid-Atlantic ridge plate boundary, where the Reykjanes ridge rises above sea level. It is an oblique spreading segment with characteristics of both divergent and transform-type plate boundaries (e.g. Saemundsson, 1978; Clifton and Schlische, 2003; Sigmundsson, 2006). The activity at Reykjanes Peninsula initiated together with the Western Volcanic Zone after a ridge jump to the east approximately 6–7 Ma, terminating the southern part of the Snæfellsnæs rift (Jóhannesson, 1980). The peninsula contains eruptive fissure swarms arranged en echelon. Based on high-temperature geothermal areas, magnetic anomalies and eruptive centers, the peninsula has been divided into five different volcanic systems: Hengill, Brennisteinfjöll, Krísuvík, Svartshengi and Reykjanes. However, based on petrology and major element geochemistry, Svartshengi and Reykjanes are hardly distinguishable and are often classified as one single system (the Reykjanes volcanic system) (e.g. Jakobsson et al., 1978; Einarsson and Saemundsson, 1987; Sigmundsson, 2006). Each system is about 15–40 km long by 7–15 km wide with an average strike of 040° and has eruptive fissures in the central part and non-eruptive fissures on the periphery (e.g. Saemundsson, 1978; Walker, 1993). The geometry of the volcanic systems are the surface manifestation of elongated magma reservoirs at the base of the crust (Gudmundsson, 1995), while their main topographic characteristics are controlled by the influence of the Icelandic hotspot and Pleistocene glaciations. Overall, from west to east there is a ca. 600 m increase in topography representing the increasing influence of the Iceland hotspot, which is centered under the northwestern part of the Vatnajökull ice cap (e.g. Sigmundsson, 2006). The impact of glaciations on the topography is quite complex, since glaciers change the eruptive environment and partly control the resulting volcanic landforms. Therefore, local topographic variations within each volcanic system are mainly controlled by the timing of eruption with regards to glaciations.

### 2.1. Postglacial activity: shields and fissures

Reykjanes is mostly covered by basaltic lava flows that erupted after the termination of the last glaciation, estimated at around 12,000–15,000 yr ago (e.g. Jakobsson et al., 1978; Saemundsson et al., 2010). The axial centers of the volcanic systems are dominated by eruption fissures, while shield volcanos lie on the periphery of each swarm (Jakobsson et al., 1978). The shields have near-circular plan shapes and are generally composed of pahoehoe lava flows that build up a central low-sloping lava cone surrounded by an apron (e.g. Fig. 3A–D). The ratio of apron area versus cone area varies between 3:4 and 20:1 (Rossi, 1996). The aprons have lower slopes than the cones and are often covered by flows from neighboring volcanoes, making it difficult to estimate their actual size. The central cones contain variably developed summit craters. The shields are thought to be monogenetic and in some cases parasitic to larger shields (Rossi, 1996; Andrew and Gudmundsson, 2007). They erupted during early postglacial times and are divided into picrite and olivine tholeiite lava shields, where the smaller volume picrite shields are believed to have preceded the more extensive olivine tholeiite shields, which probably formed during long-lived eruptions (Jakobsson et al., 1978). The younger eruptive activity was dominated by fissure eruptions concentrated along the axis of the volcanic systems, producing disconnected small volumes of slag or rows of scoria cones often with a'a lavas (Jakobsson et al., 1978; Gudmundsson, 1986). The fissure eruptions were presumably short-lived, high effusion rate eruptions and are the youngest postglacial eruptive products; the last known eruption occurred in the thirteenth century (Saemundsson et al., 2010).

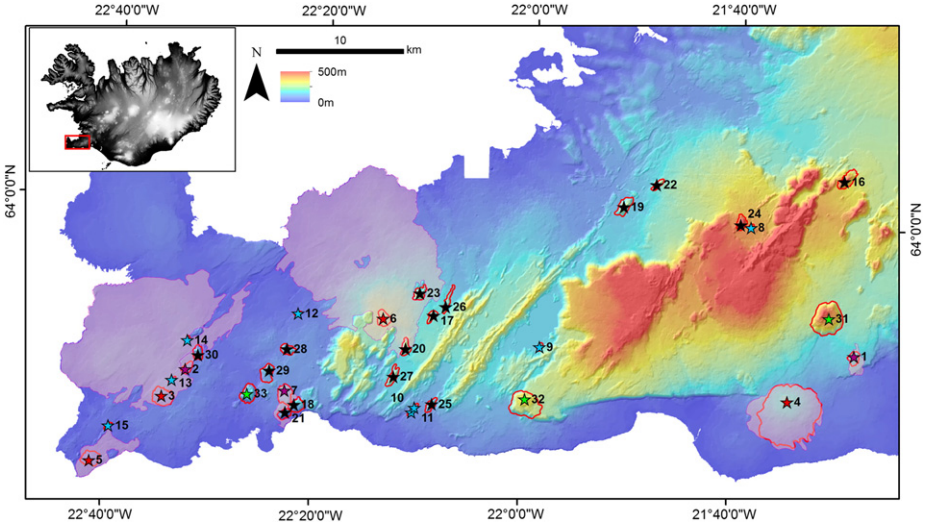


**Fig. 2.** DEM-derived topographic map of the Reykjanes Peninsula ranging from 0 m (blue) to 500 m (red). The stars denote the location of each of the 33 analyzed volcanic edifices (class A1: red, class A2: purple, class B group 1: blue, class B group 2: black, class B group 3: green). Each edifice is numbered according to the ID number in Table 1. The red outlines are the concave edifice boundaries (CEB) and the shaded areas are the geologic boundaries (GB) for class A edifices defined by Saemundsson et al. (2010). Inset is a DEM of Iceland showing location of the study area.

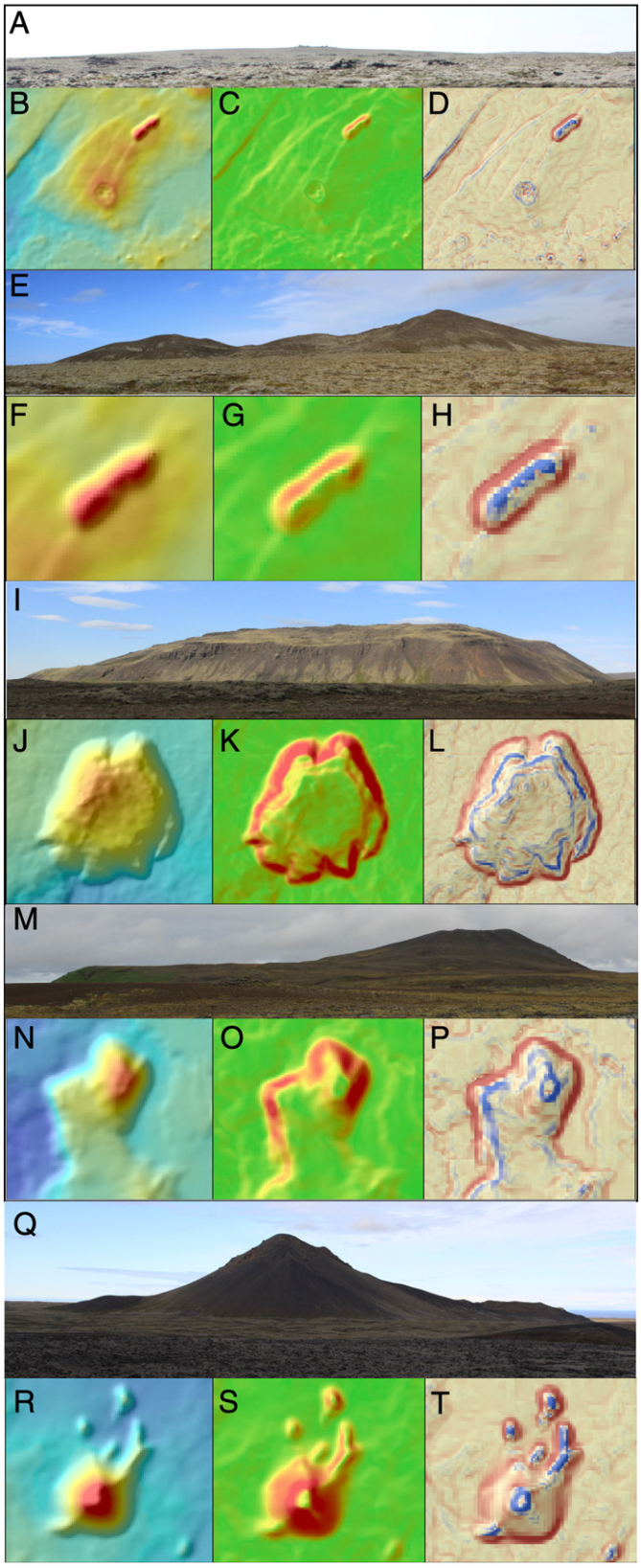


**Fig. 3.** Five examples of analyzed volcanic edifices represented by a profile view the edifice from the field and three maps of topography, slope and profile curvature. The slope maps range from green (0°) to red (30°) and the profile curvature maps range from blue (−4) to red (4). The elevation scale for the topographic maps varies from edifice to edifice. (A–D) Sandfellsdalur, an olivine tholeiitic shield. Map view is 40 km across. (E–H) Sandfell W, a tindar. Map view is 12 km across. (I–L) Geitafell, a flat-topped tuya. Map view is 36 km across. (M–P) Syllingafell, a complex tuya. Map view is 20 km across. (Q–T) Keilir, a conical tuya. Map view is 20 km across.

**Table 1**
Morphometric parameters for the 33 studied volcanic edifices. The landform type is classified following Russell et al. (2014). Column 'Unit' contains the unit description of each edifice based on Saemundsson et al. (2010) and Saemundsson (personal communication). Column "Age" is based on the map of Saemundsson et al. (2010). Column "Notes" contains information on post-emplacement modification such as faulting (based on Clifton and Schlische, 2003, and Saemundsson et al., 2010) and observations of glacial stria (based on Kjartansson, 1960).

| Class | Group | ID number | Volcanic edifice | Location | Height (m) | Basal area ($km^2$) | Summit area ($km^2$) | Basal width (km) | Summit width (km) | Volume ($km^3$) | Mean slope (°) | Average elongation azimuth (°) |
|---|---|---|---|---|---|---|---|---|---|---|---|---|
| A2 | – | 1 | Búrfell | 21°28′14 W; 63°54′41 N | 64 | 0.704 | 0.292 | 0.95 | 0.61 | 0.0114 | 6.5 | 23 |
| A2 | – | 2 | Lágafell | 22°32′26 W; 63°52′49 N | 39 | 0.538 | 0.026 | 0.83 | 0.18 | 0.0073 | 5.6 | 24 |
| A1 | – | 3 | Sandfellsdalur | 22°34′35 W; 63°51′38 N | 50 | 1.796 | 0.343 | 1.51 | 0.66 | 0.0197 | 3.3 | 175 |
| A1 | – | 4 | Selvogsheidi | 21°34′29 W; 63°52′39 N | 176 | 18.134 | 0.401 | 4.81 | 0.71 | 0.6402 | 3.2 | 96 |
| A1 | – | 5 | Skálafell | 22°41′11 W; 63°48′44 N | 62 | 1.288 | 0.016 | 1.28 | 0.14 | 0.0187 | 4.6 | 109 |
| A1 | – | 6 | Thrainsskjaldarhraun | 22°15′59 W; 63°57′58 N | 23 | 0.953 | 0.563 | 1.10 | 0.85 | 0.0061 | 2.8 | 156 |
| A2 | – | 7 | Vatnsheidi | 22°22′49 W; 63°52′8 N | 56 | 1.362 | 0.532 | 1.32 | 0.82 | 0.0228 | 5.3 | 171 |
| B | 1 | 8 | Drottning | 21°38′37 W; 63°59′57 N | 88 | 0.140 | 0.005 | 0.42 | 0.08 | 0.0036 | 20.0 | 40 |
| B | 1 | 9 | Geithöfdi | 21°58′30 W; 63°54′31 N | 78 | 0.201 | 0.074 | 0.51 | 0.31 | 0.0065 | 18.4 | 17 |
| B | 1 | 10 | Latsfjall N | 22°10′16 W; 63°51′42 N | 50 | 0.141 | 0.016 | 0.42 | 0.14 | 0.0016 | 12.4 | 49 |
| B | 1 | 11 | Latsfjall S | 22°10′32 W; 63°51′3 N | 73 | 0.118 | 0.003 | 0.39 | 0.06 | 0.0020 | 15.9 | 46 |
| B | 1 | 12 | Litla-Skógsfell | 22°21′53 W; 63°55′26 N | 49 | 0.113 | 0.021 | 0.38 | 0.16 | 0.0016 | 14.8 | 62 |
| B | 1 | 13 | Sandfell W | 22°33′41 W; 63°52′02 N | 56 | 0.146 | 0.052 | 0.43 | 0.26 | 0.0027 | 16.1 | 50 |
| B | 1 | 14 | Súlur | 22°32′23 W; 63°54′3 N | 77 | 0.118 | 0.007 | 0.39 | 0.10 | 0.0028 | 22.0 | 25 |
| B | 1 | 15 | Sýrfell | 22°39′32 W; 63°50′15 N | 75 | 0.198 | 0.003 | 0.50 | 0.07 | 0.0046 | 18.4 | 45 |
| B | 2 | 16 | Blákollur | 21°29′47 W; 64°2′3 N | 265 | 1.278 | 0.011 | 1.28 | 0.12 | 0.0719 | 18.8 | 48 |
| B | 2 | 17 | Driffel | 22°8′50 W; 63°55′38 N | 82 | 0.448 | 0.020 | 0.76 | 0.16 | 0.0111 | 14.4 | 25 |
| B | 2 | 18 | Fiskidalsfjall | 22°21′49 W; 63°51′34 N | 175 | 0.955 | 0.018 | 1.10 | 0.15 | 0.0500 | 16.6 | 58 |
| B | 2 | 19 | Helgafell | 21°11′11 W; 64°0′36 N | 230 | 1.176 | 0.030 | 1.22 | 0.20 | 0.0822 | 22.1 | 33 |
| B | 2 | 20 | Hraunssels-Vatnsfell | 22°11′23 W; 63°54′10 N | 111 | 0.685 | 0.102 | 0.93 | 0.36 | 0.0240 | 15.2 | 177 |
| B | 2 | 21 | Húsafell | 22°22′38 W; 63°51′13 N | 158 | 0.623 | 0.008 | 0.89 | 0.10 | 0.0249 | 16.7 | 62 |
| B | 2 | 22 | Húsfell | 21°47′55 W; 64°1′36 N | 129 | 0.404 | 0.056 | 0.72 | 0.27 | 0.0141 | 20.7 | 49 |
| B | 2 | 23 | Keilir | 22°10′15 W; 63°56′33 N | 225 | 0.773 | 0.004 | 0.99 | 0.07 | 0.0362 | 20.0 | 5 |
| B | 2 | 24 | Kóngsfell | 21°39′38 W; 64°0′3 N | 209 | 0.708 | 0.004 | 0.95 | 0.07 | 0.0448 | 22.1 | 29 |
| B | 2 | 25 | Krýsuvikur-Mælifell | 22°8′37 W; 63°51′53 N | 137 | 0.547 | 0.006 | 0.83 | 0.09 | 0.0177 | 16.5 | 36 |
| B | 2 | 26 | Oddafell | 22°7′42 W; 63°56′2 N | 92 | 0.593 | 0.171 | 0.87 | 0.47 | 0.0109 | 13.7 | 17 |
| B | 2 | 27 | Sandfell E | 22°12′25 W; 63°52′58 N | 144 | 0.796 | 0.121 | 1.01 | 0.39 | 0.0303 | 18.4 | 32 |
| B | 2 | 28 | Stóra-Skógsfell | 22°22′46 W; 63°53′54 N | 125 | 0.716 | 0.293 | 0.95 | 0.61 | 0.0246 | 15.9 | 105 |
| B | 2 | 29 | Syllingarfell | 22°24′22 W; 63°52′57 N | 165 | 1.130 | 0.040 | 1.20 | 0.23 | 0.0447 | 13.4 | 9 |
| B | 2 | 30 | Thórdafell | 22°31′17 W; 63°53′27 N | 130 | 0.706 | 0.353 | 0.95 | 0.67 | 0.0243 | 15.0 | 161 |
| B | 3 | 31 | Geitafell | 21°30′47 W; 63°56′15 N | 355 | 4.939 | 0.038 | 2.51 | 0.22 | 0.6385 | 16.9 | 44 |
| B | 3 | 32 | Geitahlid | 21°59′43 W; 63°52′17 N | 274 | 3.862 | 0.199 | 2.22 | 0.50 | 0.3076 | 13.1 | 78 |
| B | 3 | 33 | Thorbjörn | 22°26′23 W; 63°51′55 N | 197 | 1.379 | 0.529 | 1.33 | 0.82 | 0.1046 | 19.2 | 179 |

### 2.2. Intraglacial activity: tindars and tuyas

Glaciovolcanic edifices are numerous on Reykjanes Peninsula and range from small tindars to flat-topped tuyas to multiple, polygenetic complexes of intergrown tindars and tuyas with different ages, often modified by later postglacial lava flows (Saemundsson et al., 2010). The four different examples analyzed in this study are shown in Fig. 3E–T.

The composition of the glaciovolcanic edifices is primarily basaltic, though a few andesitic tindars have been mapped in the central part of the Hengill system, such as Húsmúli and Stapafell (Saemundsson et al., 2010). A few glaciovolcanic edifices are also know to be of picritic composition and include Stapafell from the Reykjanes volcanic system and Stakihnúkur, Mælifell, and Midfell from the Hengill volcanic system (Saemundsson, personal communication).

A limited number of detailed studies have concentrated on the tindars Helgafell (Schopka et al., 2006) and Undirhlidar (Hiatt et al., 2013; Pollock et al., 2013; Was et al., 2013), and on the tindar complex Sveifluháls (Mercurio et al., 2009; Skilling et al., 2009), all from the Krísuvík volcanic system.

Helgafell is an example of a relatively small basaltic hyaloclastite tindar thought to have formed in a single eruption (Schopka et al., 2006). Gravity modeling suggests that pillow lava and intrusions make up only a few percent of the total volume, while volatile content from glass samples suggests that the eruption took place under a minimum 500 m thick ice sheet.

Undirhlidar, located 1 km west of Helgafell, is a pillow tindar with a complex 4-stage emplacement model (Pollock et al., 2013). Occurrence of the same magma composition in two different quarries suggests that a kilometer-scale fissure segment was active at multiple points (Was et al., 2013) and the volatile content in quenched glass rinds imply that the eruption took place under pressures equivalent to 450–575 m of water (Hiatt et al., 2013). Small volumes of tuff breccia suggest some explosive activity during the tindar formation, revealing that small tindars can have complex magma supply dynamics (Pollock et al., 2013).

Sveifluháls is a ca. 22 km long tindar complex that originated from at least 9 sub-parallel fissures spaced 0.1–0.5 km apart, with an average vent-spacing of 0.7 km (Mercurio et al., 2009; Skilling et al., 2009). The dominant lithology is subaqueous lavas draped by phreatomagmatic tephra, and the volatile content in pillow glass rinds constrains ice thickness between 70 and 400 m (Mercurio et al., 2009; Skilling et al., 2009).

Most glaciovolcanoes on Reykjanes Peninsula are thought to be from either Early or Late Weichsel, though some deposits are older and have been ascribed to Early Brunhes (Saemundsson et al., 2010). However, K–Ar ages of young basaltic landforms are notoriously uncertain due the long half-life of the system, the low abundance of K in the basalts and the equilibration of the Ar content with the atmosphere (Levi et al., 1990), so that all existing ages should be treated with caution (Saemundsson, personal communication).

Depending on their age, the glaciovolcanic edifices may have experienced varying degrees of post-emplacement modification due to glacial

| Basal Elongation azimuth (°) | Average E.I. | Basal E.I. | Average I.I. | Basal I.I. | Height/ basal width | Summit width/ basal width | Morphology | Unit | Area Lava cap ($km^2$) | Age | Notes |
|---|---|---|---|---|---|---|---|---|---|---|---|
| 20 | 1.46 | 1.53 | 1.02 | 1.15 | 0.05 | 0.64 | Shield | Picrite lava | | – | – |
| 36 | 1.21 | 1.91 | 1.01 | 1.11 | 0.03 | 0.22 | Shield | Picrite lava | | – | Faulted |
| 77 | 1.62 | 1.33 | 1.13 | 1.20 | 0.02 | 0.44 | Shield | Olivine tholeiite lava | | >7000 yr | Faulted |
| 54 | 1.43 | 1.33 | 1.16 | 1.27 | 0.02 | 0.15 | Shield | Olivine tholeiite lava | | >7000 yr | Faulted |
| 74 | 1.53 | 1.60 | 1.10 | 1.15 | 0.04 | 0.11 | Shield | Olivine tholeiite lava | | >2400 | Partly faulted |
| 166 | 2.14 | 1.48 | 1.30 | 1.14 | 0.01 | 0.77 | Shield | Olivine tholeiite lava | | >7000 yr | Partly faulted |
| 170 | 2.48 | 1.63 | 1.20 | 1.16 | 0.03 | 0.62 | Shield | Picrite lava | | – | Faulted |
| 35 | 2.26 | 1.94 | 1.00 | 1.06 | 0.16 | 0.18 | Tindar | Hyaloclastite | | E.W. | – |
| 24 | 2.06 | 1.81 | 1.00 | 1.06 | 0.13 | 0.61 | Tindar | Hyaloclastite with compound lava | 0.164 | E.B. | – |
| 55 | 4.74 | 2.30 | 1.06 | 1.08 | 0.08 | 0.34 | Tindar | Pillow lava | | L.W. | Partly faulted |
| 49 | 1.91 | 3.03 | 1.01 | 1.11 | 0.14 | 0.16 | Tindar | Pillow lava | | L.W. | Faulted |
| 67 | 3.47 | 2.58 | 1.04 | 1.10 | 0.10 | 0.43 | Tindar | Pillow lava | | E.W. | Partly faulted |
| 52 | 3.54 | 2.73 | 1.07 | 1.08 | 0.10 | 0.60 | Tindar | Hyaloclastite | | L.W. | Faulted |
| 23 | 2.49 | 2.13 | 1.02 | 1.12 | 0.17 | 0.25 | Tindar | Pillow lava | | L. W. | Faulted |
| 52 | 3.11 | 2.44 | 1.03 | 1.10 | 0.12 | 0.13 | Tindar | Hyaloclastite with compound lava | 0.071 | L. W. | Faulted |
| 38 | 2.86 | 2.31 | 1.03 | 1.17 | 0.14 | 0.09 | Tindar | Hyaloclastite with compound lava | 0.123 | L.W. | – |
| 30 | 3.47 | 2.41 | 1.09 | 1.15 | 0.10 | 0.21 | Complex tuya | Hyaloclastite with compound lava | 0.141 | E.B. | – |
| 67 | 2.56 | 1.35 | 1.03 | 1.14 | 0.12 | 0.14 | Complex tuya | Hyaloclastite with compound lava | 0.490 | E.W. | – |
| 48 | 2.10 | 2.41 | 1.06 | 1.14 | 0.17 | 0.16 | Tindar | Hyaloclastite | | E. W. | Faulted |
| 13 | 2.56 | 2.43 | 1.15 | 1.14 | 0.08 | 0.39 | Complex tuya | Hyaloclastite with compound lava | 0.278 | L.W. | – |
| 75 | 1.70 | 1.57 | 1.05 | 1.10 | 0.12 | 0.11 | Complex tuya | Hyaloclastite with compound lava | 0.269 | E.W.–L.W. | – |
| 53 | 4.41 | 3.21 | 1.07 | 1.13 | 0.14 | 0.37 | Tindar | Hyaloclastite | | E.W.: | Partly faulted |
| 38 | 1.34 | 2.19 | 1.03 | 1.21 | 0.20 | 0.07 | Conical tuya | Hyaloclastite with compound lava | 0.020 | E.B. | – |
| 10 | 1.85 | 1.87 | 1.03 | 1.09 | 0.16 | 0.07 | Complex tuya | Hyaloclastite with compound lava | 0.199 | E.W. | Partly faulted |
| 38 | 2.12 | 2.80 | 1.00 | 1.12 | 0.14 | 0.10 | Complex tuya | Pillow lava | | L.W. | – |
| 20 | 9.09 | 7.49 | 1.19 | 1.22 | 0.04 | 0.54 | Tindar | Pillow lava | | L.W. | – |
| 22 | 4.26 | 3.50 | 1.05 | 1.28 | 0.12 | 0.39 | Tindar | Hyaloclastite | | L.W. | – |
| 106 | 2.30 | 1.71 | 1.28 | 1.13 | 0.11 | 0.64 | Complex tuya | Pillow lava | | E.W. | Faulted |
| 177 | 1.52 | 1.57 | 1.06 | 1.16 | 0.10 | 0.19 | Complex tuya | Hyaloclastite with compound lava | 0.767 | L.W. | Faulted |
| 169 | 1.63 | 1.67 | 1.18 | 1.14 | 0.12 | 0.71 | Complex tuya | Pillow lava | | E.B. | Faulted |
| 22 | 1.67 | 1.31 | 1.08 | 1.13 | 0.10 | 0.09 | Flat-topped tuya | Hyaloclastite with compound lava | 2.475 | E.W. | Faulted. Glacial stria |
| 86 | 1.61 | 1.40 | 1.09 | 1.16 | 0.08 | 0.23 | Flat-topped tuya | Hyaloclastite with compound lavas | 2.461 | E.–L. W. | – |
| 21 | 1.35 | 1.44 | 1.06 | 1.13 | 0.14 | 0.62 | Flat-topped tuya | Pillow lava | | E.B. | Heavily faulted |

erosion. However, the effect of glacial erosion is difficult to quantify due to the limited studies. Schopka et al. (2006) concluded that Helgafell has not suffered major erosion, while the other above mentioned studies have not addressed the extent of glacial erosion. Glacial striations are marked in the 1:250.000 map of Kjartansson (1960), but this provides only information on glacial erosion of lavas since striations are not well-preserved in fine-grained volcaniclastic deposits. The only edifice with glacial stria that we analyze here is Geitafell. Faulting may also play a role in modifying the edifices, depending on their location within the volcanic system; edifices such as Thorbjörn and Thórdafell are cross-cut by multiple faults (Clifton and Schlische, 2003; Saemundsson et al., 2010, Table 1).

## 3. Data & methods

We have used a 20 m spatial resolution DEM based on photogrammetry of aerial images from the company Loftmyndir ehf. It is the best DEM available for the entire area. This resolution does not allow identification of small landforms such as lava flows and fissure swarms. However, it is adequate for morphometric studies of topographically distinct volcanic landforms down to ~0.1 $km^2$ (i.e. 250 pixels). We therefore selected volcanic edifices with bases larger than 0.1 $km^2$ and with distinct positive topographies. From these, we discarded (1) edifices substantially covered by more recent deposits, (2) edifice complexes with unclear topographic boundaries, and (3) edifices assigned to different ages by Saemundsson et al. (2010). Based on these criteria, we analyzed 33 edifices from the Reykjanes, Krísuvík, Brennisteinfjöll and Hengill volcanic systems (Fig. 2, Table 1), consisting of 7 subaerial shields and 26 glaciovolcanoes that are relatively simple, with no or minor cross-cutting relationships, and that likely formed during a single event (i.e. monogenetic).

To characterize the volcanic edifices morphometrically, we used the methodology presented by Grosse et al. (2009, 2012). The systematic extraction of morphometric parameters relies on the spatial delimitation of each analyzed volcanic edifice. Delimiting a volcano is a difficult and non-trivial task, partly because the topography of volcanoes is influenced by the surrounding landforms, but also because volcanic products can be buried or deposited far away. We have used the concave edifice boundary (CEB) delimitation method described in Grosse et al. (2012). This method is solely based on topography and the boundary is defined at concave breaks in slope around the edifice base. Since this method only considers the edifices, it omits far reaching volcanic products such as lava aprons, lahars and ash, and it therefore underestimates the total volume of the volcano and its products. However, the method has the advantage of being a consistent and objective approach that can enable comparisons of a variety of volcanic landforms on a uniform basis.

The geomorphic parameters were computed from the DEM and the defined edifice boundary using the IDL-language MORVOLC code (Grosse et al., 2012). The basal width and area are directly derived from the edifice boundary, which is also used to compute height and volume by fitting a 3D base using an inverse distance weighting interpolation. Plan shape parameters are calculated from the basal outline and from the closed elevation contour lines (at 10 m equidistance) above the edifice boundary; they consist of the ellipticity index (basal E.I. and average E.I.), which quantifies edifice elongation, and the irregularity index (basal I.I. and average I.I.), which quantifies edifice complexity (for details see Grosse et al., 2012). The basal E.I. value is equivalent to

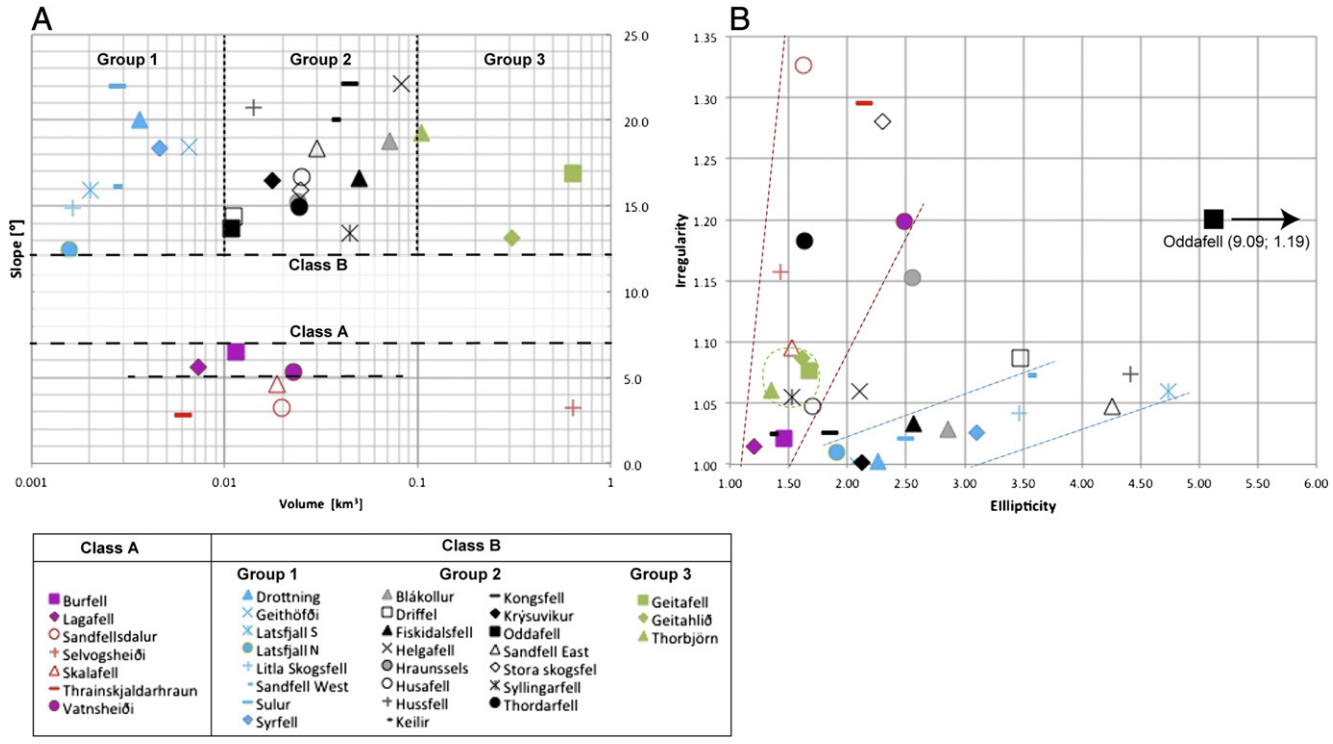


**Fig. 4.** Two diagrams displaying (A) average slope versus volume, and (B) average irregularity versus average ellipticity. In (A) edifices are classified into classes and subclasses based on slope and into groups based on volume. In (B) class A (red), class B group 1 (blue) and class B group 3 (green) cluster in fields with specific ellipticity and irregularity, but there is considerable overlap, specially with class B group 2.

the basal length to width ratio used in other studies. Slope values are directly derived from the DEM and are used to compute average slopes, slope histograms and slopes as a function of height.

The CEB outlines of the glaciovolcanic edifices fit the geologic map of Saemundsson et al. (2010) quite well. The outline delimitation of the shallow-sloping shields is more problematic because breaks in slope are extremely subtle; the CEB outlines tend to include only the central cones and discard most of the surrounding lava aprons. Therefore, the CEB-derived spatial extents of the shields are significantly smaller than outlined on the geologic map of Saemundsson et al. (2010). To be able to compare to previous studies (Jakobsson et al., 1978; Rossi, 1996) and to evaluate the impact of the CEB method on the morphometric parameters, the MORVOLC code was run twice for the shields; once using the CEB outline and once using the geologic boundaries (GB) from Saemundsson et al. (2010) (Fig. 2). Thus, all 33 edifices were analyzed using the CEB outline, and the 7 shields were also analyzed using the GB outline. It should be noted that all volume estimates are prone to underestimate the actual eruption volume, since the edifice may be buried under newer deposits. This is typically the case for glaciovolcanic edifices that later acted as topographic barriers diverting younger lava flows.

We use the geologic map of Saemundsson et al. (2010) to uniformly compare the geologic data with the morphometric results from the 33 analyzed edifices. Hence, we have mainly incorporated the map terminology for geologic units. In the map, the glaciovolcanic edifices are divided into two lithological units, lava caps and hyaloclastite. We have added an additional category of pillow lava (obtained from Saemundsson, personal communication) in order to asses if hyaloclastite-dominated tindars are morphometrically different from pillow lava-dominated tindars. Hence, we use hyaloclastite as a general term for hyalotuff, hyaloclastite, lapilli tuff and tuff-breccia. All of the analyzed glaciovolcanic edifices are of basaltic composition, therefore no compositional distinction is possible. The subaerial shields are distinguished in the map according to composition into 'picrite lavas' and 'other lavas'. Of the 7 shields we have analyzed, 3 are picritic and the other 4 fall in the 'other lavas' category, and are known to be olivine tholeiite shields (Jakobsson et al., 1978; Rossi, 1996).

## 4. Results: morphometric characteristics of volcanic edifices

The analyzed edifices (Fig. 2) represent a wide spectrum of landforms. The results of the morphometric analysis are divided into three parts. First, the edifices are characterized and classified according to the morphometric parameters calculated using the CEB outlines, and compared to the geologic map of Saemundsson et al. (2010). Subsequently, the morphometric data for the shields using the CEB and GB delimitations are compared in order to evaluate the strength of the classification. Finally, morphometric trends are evaluated in order to resolve the impact of individual landform elements, where a landform element is defined as the smallest unit, indivisible at the given resolution, bounded by topographic continuities and with relatively uniform morphometry (Pike et al., 2009).

### 4.1. Morphometric signature of volcanic landforms

The 33 edifices can be divided into 2 classes based on average slopes (Fig. 4, Table 1): low sloping edifices (class A) and steep sloping edifices (class B). Class A contains seven edifices that correspond to lava shields produced under subaerial conditions, whereas class B contains 26 glaciovolcanic edifices (Table 2).

#### 4.1.1. Morphometry of subaerial shields

Class A contains seven shield-shaped edifices that are remarkably different from class B edifices; they have average slopes ranging from 2.8° to 6.5°, whereas class B edifices have average slopes >12° (i.e. a slope gap of over 5°; Fig. 3a). Furthermore, class A can be divided into two subclasses also using average slopes; subclass A1 with average slopes <5° and subclass A2 with average slopes >5° (Fig. 4a), which correspond to olivine tholeiitic shields (4 edifices) and picrite shields

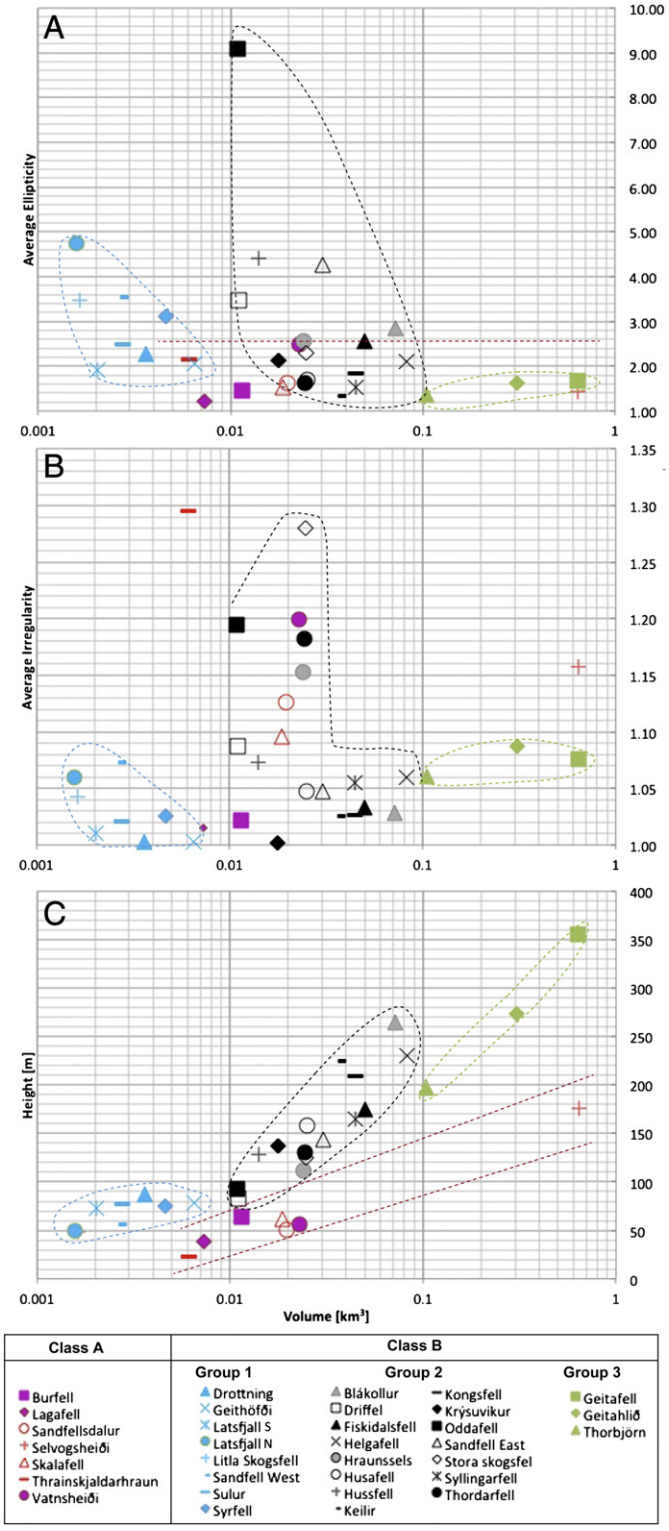


**Fig. 5.** Diagrams showing (A) ellipticity, (B) irregularity, and (C) height of edifices as a function of volume.

(3 edifices), respectively. However, this is a tentative sub-classification due to the low number of edifices in each subclass.

Except for very large Selvogsheidi, the edifices of class A have sizes that range from 0.006 to 0.023 $km^3$ in volume, 0.8 to 1.5 km in basal width and 23 to 64 m in height (Table 1). These values overlap mostly with the sizes shown by group 2 in class B, though their heights are the lowest of all edifices, partially overlapping with those of group B1 (see below, Fig. 5).

The average and basal E.I. and I.I. indicate that class A edifices are fairly circular (low E.I.) and have variable irregularity (Figs. 4–5, Table 2).

*4.1.2. Morphometry of glaciovolcanic edifices*

Class B edifices have average slopes ranging from 12.4° to 22.1°. Within class B there are vast differences in size and shape, and to resolve these differences, the class was divided into 3 groups based on size

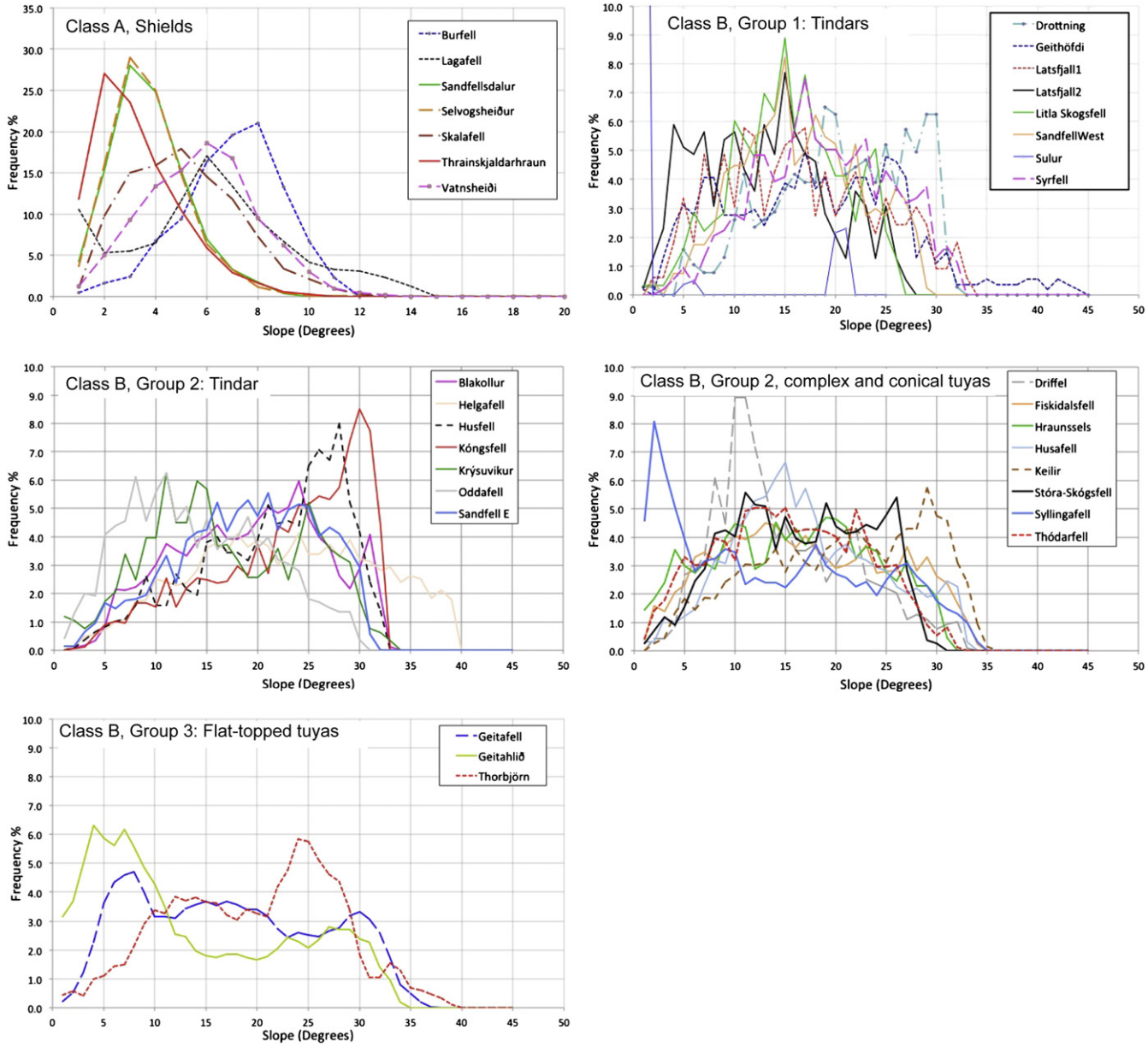


**Fig. 6.** Slope frequency histograms for each class (class A: Subaerial shields, class B: Glaciovolcanic edifices) and group (1–3). Note that the axes for class A are different from those of class B and that class B, group 2 has been divided into two diagrams.

(basal width, area and volume) (Fig. 4a). Average slopes between the 3 groups overlap significantly (Fig. 4a) with values ranging from 12.4° to 22.0° for group 1, 13.4° to 22.1° for group 2, and 13.1° to 19.2° for group 3. The average and basal E.I. and I.I. values show some differences between the groups, but they are not strictly diagnostic as there is overlap (Fig. 4b).

Group B1 consists of eight linear ridges which can be classified as tindars following Russell et al. (2014). These edifices are the smallest in terms of volume (0.0016–0.0065 km$^3$) and basal width (0.38–0.51 km), and have, together with class A, the lowest heights (49–88 m, Table 2). They are strongly elongated, with average and basal E.I. >1.8, (most > 2), and they are quite regular, with I.I. values mostly < 1.1 (Figs. 4b–5, Table 1). All eight edifices have elongation azimuths between 20 and 70°N (Table 2).

Group B2 contains 15 edifices and displays the greatest variety in shape ranging from fairly linear to more equidimensional and complex edifices (Figs. 4b–5). They can be classified as tindars (7 edifices), conical tuyas (1 edifice) and complex tuyas (7 edifices) following Russell et al. (2014) (Table 1). The edifices are intermediate in size, with volumes from 0.0111 to 0.0822 km$^3$ and basal widths between 0.72 and 1.28 km. Heights (82–265 m) show some overlap with groups B1 and B3. This group shows the greatest spread in E.I. and I.I. (Figs. 4b–5, Table 2). Tindars have relatively high E.I. and low I.I., similar to group B1, whereas complex tuyas have very variable I.I., but there is overlap and a quantitative separation is not straightforward. Keilir, the only conical tuya in our analysis, has very low E.I. and I.I. values.

Group B3 consists of three table-shaped mountains that can be classified as flat-topped tuyas following Russell et al. (2014). They have volumes between 0.1046 and 0.6385 km$^3$, which is one order of magnitude larger than group B2 and two orders larger than group B1. The edifices are also significantly larger in basal area, having values a magnitude greater than group B2 (see Table 2), while heights (197–335 m) show some overlap with group B2. They are fairly circular (low E.I. values) and quite regular (low I.I. values) and have large summit regions (Figs. 4b–5, Table 2) (Table 1).

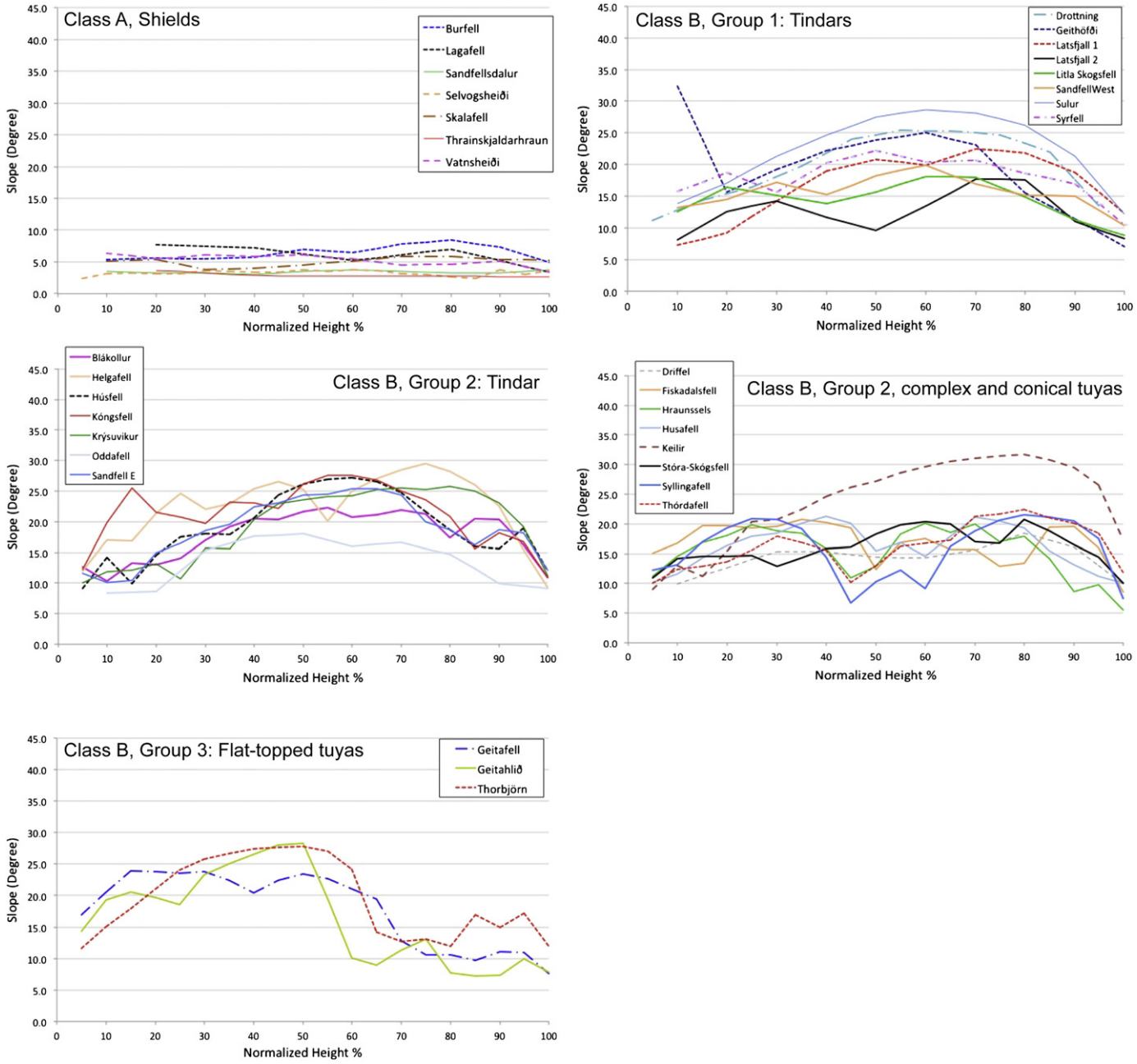


**Fig. 7.** Diagrams showing the slope values versus normalized height for each class (class A: Subaerial shields, class B: Glaciovolcanic edifices) and group (1–3). Note that class B, group 2 has been divided into two diagrams.

### *4.2. Strength of geomorphometric classification*

As mentioned in Section 3, the CEB outlines omit distal volcanic products. In order to evaluate how these omissions influence our morphometric classification, the area delineated by the CEB outlines were compared to the areas of the volcanoes as delineated on the geologic map of Saemundsson et al. (2010) (Table 3). Class A shows significant differences in edifice outlines and consequently the calculated areas have CEB/GB ratios ranging from 1 to 80%, while class B shows quite good correspondence. A few exceptions are edifices that have been partly superposed by later fissure eruptions such as Geitahlid and Syllingarfell, edifices that are segmented into separate hills such as Oddafell, Latsfjall S and Keilir, or edifices that have been mined (Súlur). The discrepancy for class A is expected because the CEB method omits the distal lava apron and basically only delimits the cone of the lava shield, whereas the geologic map delineates the entire shield.

To examine how the omission of the lava apron would influence the morphometric classification, the same morphometric analysis was carried out for the class A shields but with boundaries based on the GB method (Fig. 2, Table 4). As expected, the size parameters increase significantly using the GB delimitation, whereas the average slopes decrease. The average slope values using the GB delimitation range from 1.8° to 5.5°, with the olivine tholeiite shields between 1.8° and 2.9° and the picrite shields between 3.8° and 5.5°. Thus, the division of classes A and B based on average slope is still valid, independent of the delimitation method, as is the subdivision into subclasses A1 and A2. Moreover, since the shields are not grouped according to size, the increase in size does not affect the classification.

**Table 2**
Summary of geomorphic characteristics for classes A and B, and their subclasses and groups. The last column indicates the types of landforms within each group based on the map of Saemundsson et al. (2010).

| Class | Group | Size | | | | | Shape | | | Slope | | Landform (#) |
|---|---|---|---|---|---|---|---|---|---|---|---|---|
| | | Height (m) | Basal area ($km^2$) | Basal width (km) | Volume ($km^3$) | General | Average E.I. (basal E.I.) | Average I.I. (basal I.I.) | General | Mean slope (°) | General | |
| A | | 23–176 | 0.538–18.134 | 0.83–4.81 | 0.0061–0.6402 | Big spread of A, D and Vol., but low height. | 1.21–2.48 (1.33–1.91) | 1.01–1.30 (1.11–1.27) | Approximately equidimensional | 2.8–6.5 | Low sloping | Lava shield (7) |
| A1 | | 23–176 | 0.953–18.134 | 1.10–4.81 | 0.0061–0.6402 | Bigger | 1.43–2.14 (1.33–1.60) | 1.10–1.30 (1.11–1.16) | | 2.8–4.6 | <5° | Olivine tholeiite (4) |
| A2 | | 34–64 | 0.538–1.362 | 0.83–1.32 | 0.0073–0.0228 | Smaller | 1.46–2.48 (1.53–1.91) | 1.01–1.20 (1.14–1.27) | | 5.3–6.5 | [5;7]° | Picrite (3) |
| | 1 | 49–88 | 0.113–0.201 | 0.38–0.51 | 0.0016–0.0065 | Minimum A, D and Vol. However, higher than most edifices in (1) | 1.91–4.74 (1.81–3.03) | 1.00–1.06 (1.06–1.12) | Regular linear ridges | 12.4–22.1 | Steep slopes | Tindar (8) |
| | 2 | 82–265 | 0.404–1.278 | 0.72–1.28 | 0.0111–0.0822 | Values for W, H, A, and V are between (2) & (3) | 1.34–9.09 (1.35–7.49) | 1.00–1.28 (1.10–1.28) | Diverse | 13.1–22.0 | Steep slopes | Tindars, conical tuya and complex tuyas (15) |
| | 3 | 197–355 | 1.379–4.939 | 1.33–2.51 | 0.1046–0.6385 | Highest and biggest edifices. | 1.35–1.67 (1.31–1.44) | 1.06–.108 (1.13–1.16) | Approximately equidimensional | 13.4–16.4 | Steep flanks (10–30°) and low sloping summit/center (10°) | Flat-topped tuya (3) |

### 4.3. Morphometric impact of landform elements: trend analysis

To understand geomorphometric information for each class, subclass and group, the variety and impact of individual landform elements have to be evaluated.

Slope histograms (Fig. 6) of class A edifices show a narrow and unimodal distribution ranging from 0 to 15°, and all seven edifices have maximum slope frequencies between 2 and 8°. The two subclasses are well separated, with subclass A1 having maximum frequencies between 2 and 5°, and subclass A2 between 6 and 8°. class B edifices show more complex slope distributions. Most of group B1 edifices have irregular and unimodal distributions, with the exception of Súlur. Likewise, the majority of edifices in group B2 display irregular and unimodal slope distributions. However, their distributions tend to be wider and a few edifices have distinct maxima at low (Syllingarfell at 3°; Driffel at 10–11°) or high slopes (between 25 and 30°; Húsfell, Kóngsfell and Keilir). Group B3 edifices have broad bimodal slope distributions; Geitafell and Geitahlid have maxima between 4 and 8° and between 27 and 30°, while Thorbjörn has maxima at 12–14° and 24–25°.

The slope histograms are slope frequency distributions of all pixels within the boundary of the respective edifices. Landforms that primarily consist of one landform element (at the given resolution of the DEM) are therefore expected to have a unimodal and fairly narrow slope distribution such as observed for class A. On the other hand, landforms consisting of significantly different landform elements may be bimodal, trimodal or show broad and irregular slope distributions caused by slope overlap between landform elements. This seems to be the case for all three groups of class B.

To examine this overlap in slope, its development as a function of height was investigated (Fig. 7). For comparison, heights were normalized. Class A shows slope values ranging from 2 to 8.5°, generally increasing with height, while class B again is more complex. Edifices in group B1 show a wide, mostly smooth, parabola trend with maximum slopes at 50–80% height (with high slope values at the base of Geithöfdi as an exception). A few edifices in group B2 show a similar parabola trend as group B1, such as Keilir and Krýsivikur-Mælifell, but most edifices of the group have more irregular slope trends, with values mostly between 15 and 25° except at the base and summit regions, where they tend to be lower. Finally, edifices in group B3 show a very distinct two-step trend with highest slope values (20–30°) in the lower edifice, <50–60% height, followed by a significant lowering in slope to 7–15° at the upper edifice.

#### 4.3.1. Landforms and landform elements

Edifice morphometries were compared to the geologic map of Saemundsson et al. (2010) as well as aerial photographs in order to relate the slope properties to distinct landform elements. The results are summarized in Fig. 8.

Class A edifices are shields with very uniform and low slope values, suggesting that they consist mainly of one landform element. For subclass A1 this landform element is the olivine tholeiite lava cone, while for subclass A2 it is the picrite lave cone. Because the slope values are fairly constant the topographic profiles of the lava cone approximates a straight line (Fig. 8, first row). However, close to the summits, slopes tend to either decrease or increase depending on the size and morphology of the summit craters. Thus, summit craters are only weakly resolved by the DEM as a separate landform element (marked with parenthesis in Fig. 8, row 1). A higher resolution DEM would be necessary to quantify crater morphology.

Edifices of class B commonly have tilted bases, since they acted as topographic barriers that diverted later lava flows. This complicates the analysis of slope as a function of height because the landform elements are at different heights on either side of the edifice and thus their slope values are partially superimposed in the slope vs height graphs.

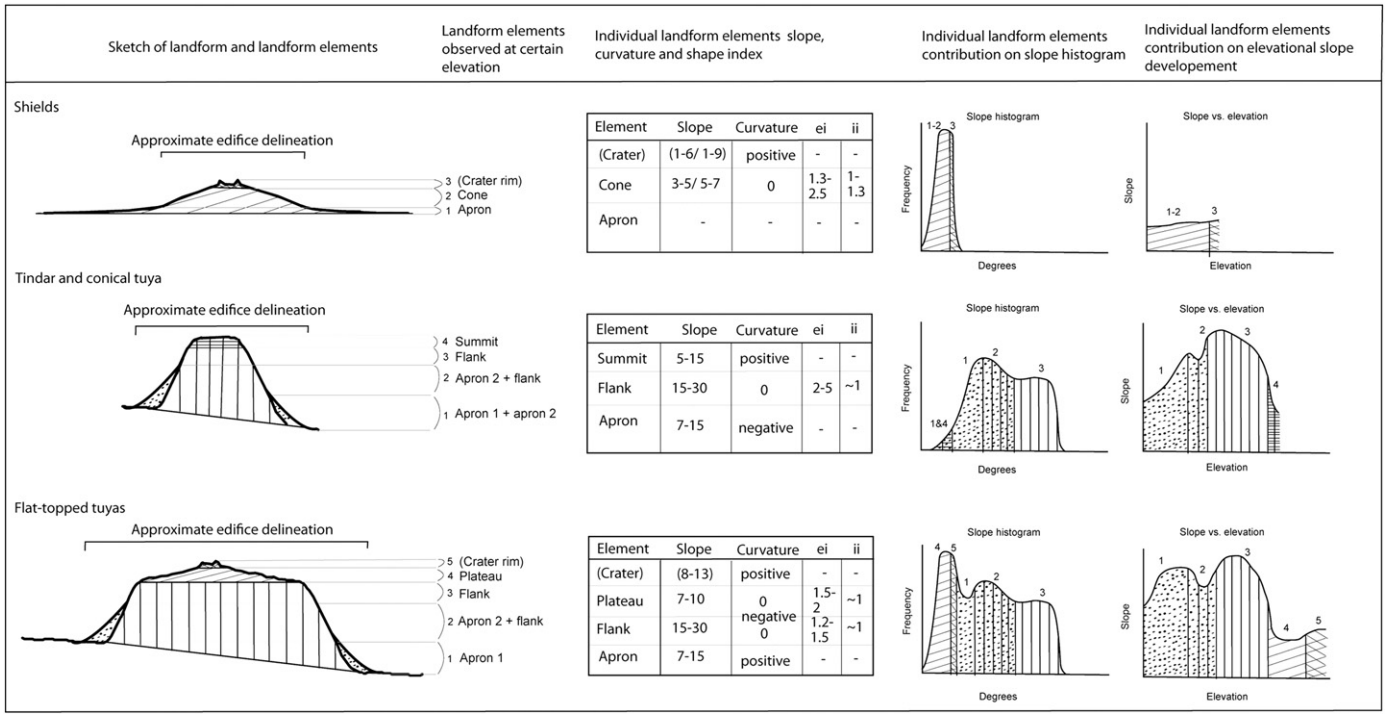


**Fig. 8.** Morphometric characteristics of subaerial shields (row 1), tindars and conical tuyas (row 2) and flat-topped tuyas (row 3), and their respective landform elements as resolved by the 20 m resolution DEM. The first column shows a profile sketch of each type of edifice with its landform elements and the approximate edifice boundary based on the CEB method. The second column displays the elevation range where each landform element is found. Column 3 gives the range of slope, curvature and E.I. and I.I. index values for each landform element. The last two columns show the contribution of each landform element on the slope frequency and slope versus elevation graphs.

Group B1 contains the simplest edifices of class B consisting of small tindars made of hyaloclastite and pillow lavas, with the exceptions of Sýrfell and Geithöfdi that also have small lava caps at their summits (Saemundsson et al., 2010, Table 1). Topography and slopes of these tindars show two discontinuities from base to summit and thus three landform elements can be considered: apron, flank and summit (Fig. 8, 2nd row). The lowermost landform element has moderate slopes (7–15°) and a concave up topographic profile. Aerial photographs show that this landform element approximately coincides with the steeper part of the apron (the lower part of the apron is omitted by the CEB method). The flank is the steepest landform element, with slopes ranging from 15 to 30° and with a linear profile. The summit has slopes ranging between 5 and 15°, similar to the apron but with a convex topographic profile.

Group B3 consists of flat-topped tuyas having broad bimodal slope distributions and distinct changes in slope with elevation. It is possible

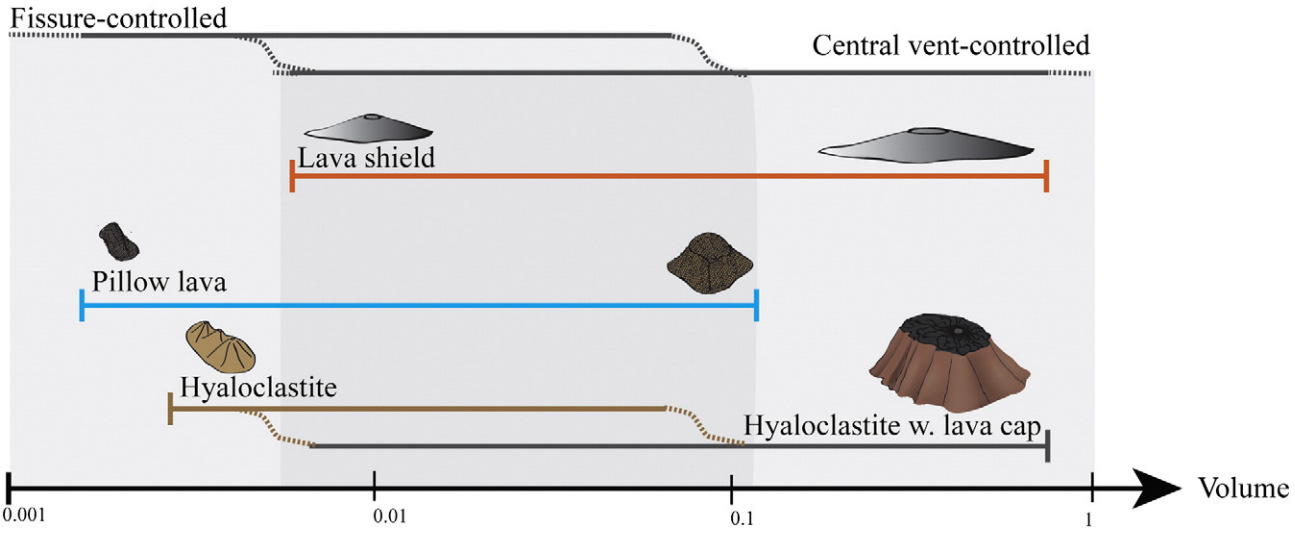


**Fig. 9.** Sketch of analyzed volcanic landforms as a function of edifice volume and dominating vent type. The volume range of fissure controlled eruptions is based on the volumetric distribution of tindars (high E.I.), while the volumetric distribution of shields, conical tuyas and flat-topped tuyas are interpreted as eruptions controlled by central vents (low E.I.). The dark gray field is the volumetric range where edifices from both fissure and circular vent eruptions are observed. The orange bar shows the volume range of lava shields. The blue bar is the volume range of edifices composed mainly of pillow lavas. The smallest pillow lava edifices are tindars whereas pillow dominated complex tuyas or pillow dominated flat-topped tuyas are observed for bigger edifices. The brown and black bars are the volume ranges of hyaloclastite tindars and flat-topped tuyas with and without a lava cap, respectively. The dashed lines indicate the interpreted transition where tindars may develop a lava cap.

**Table 3**
Comparison of the areal extent of all edifices as outlined by the concave edifice boundary (CEB) and geologic boundary (GB) delimitation methods.

| Class | Group | Edifice | CEB area ($km^2$) | GB area ($km^2$) | CEB/GB (%) |
|---|---|---|---|---|---|
| A | | Búrfell | 0.700 | 2.000 | 35.00 |
| | | Lágafell | 0.540 | 1.327 | 40.71 |
| | | Sandfellsdalur | 1.796 | 94.400 | 1.90 |
| | | Selvogsheidi | 18.134 | 22.547 | 80.43 |
| | | Skálafell | 1.288 | 7.263 | 17.73 |
| | | Thrainsskjaldarhraun | 0.953 | 102.892 | 0.93 |
| | | Vatnasheidi | 1.362 | 2.723 | 50.04 |
| B | 1 | Drottning | 0.140 | 0.140 | 100.00 |
| | | Geithöfdi | 0.201 | 0.247 | 81.39 |
| | | Latsfjall S | 0.118 | 0.202 | 58.29 |
| | | Latsfjall N | 0.141 | 0.105 | 134.06 |
| | | Litla-Skógsfell | 0.113 | 0.139 | 81.51 |
| | | Sandfell W | 0.146 | 0.146 | 100.00 |
| | | Súlur | 0.118 | 0.680 | 18.00 |
| | | Sýrfell | 0.198 | 0.204 | 97.18 |
| | 2 | Blákollur | 1.278 | 1.412 | 90.48 |
| | | Driffell | 0.448 | 0.505 | 88.73 |
| | | Fiskidalsfjall | 0.955 | 0.991 | 96.30 |
| | | Helgafell | 1.176 | 1.176 | 100.00 |
| | | Hraunssels-Vatnsfell | 0.685 | 0.612 | 111.82 |
| | | Húsafell | 0.623 | 0.760 | 81.96 |
| | | Húsfell | 0.404 | 0.548 | 73.70 |
| | | Keilir | 0.773 | 0.994 | 77.77 |
| | | Kóngsfell | 0.708 | 0.750 | 94.45 |
| | | Krýsuvikur-Mælifell | 0.547 | 0.547 | 100.00 |
| | | Oddafell | 0.593 | 0.666 | 89.08 |
| | | Sandfell E | 0.796 | 0.839 | 94.88 |
| | | Stóra-Skógsfell | 0.716 | 0.672 | 106.55 |
| | | Syllingarfell | 1.130 | 0.709 | 159.40 |
| | | Thórdafell | 0.706 | 0.738 | 95.63 |
| | 3 | Geitafell | 4.939 | 5.090 | 97.03 |
| | | Geitahlid | 3.862 | 4.951 | 78.01 |
| | | Thorbjörn | 1.379 | 1.389 | 99.30 |

to distinguish four landform elements: apron, flank, summit plateau and summit crater (Fig. 8, 3rd row). Like the tindars of group B1, the two lowermost landform elements are aprons and flanks, with similar properties as described above. There is a significant discontinuity between the flank slopes (15–30°) and the summit plateau slopes (7–15°). The summit plateau is a pillow lava plateau at Thorbjörn (10–15°), whereas at Geitafell and Geitahlid it is a lava cap (7–10°). The slopes of these lava caps are slightly higher than those of the purely subaerial lava cones of class A. Close to the summit, slope values become more irregular and seem to increase at the highest point of the edifice, mostly coinciding with the summit crater. However, as for the summit craters of class A, these summit craters are only weakly resolved by the DEM. Thus, the slope frequency histograms and slope vs height graphs can be considered a combination of class A and group B1.

The edifices in group B2 are more varied and have complex shapes and slope distributions. Some are similar to group B1, i.e. they are large tindars (e.g. Helgafell and Sandfell E), and Keilir is the only conical tuya. The other edifices are complex tuyas with characteristics of both tindars and flat-topped tuyas (e.g. Driffel and Húsafell). Group B2 is therefore an intermediate group, not only volumetrically but also morphologically.

## 5. Discussion

This study shows that a simple geomorphometric classification based on average slope easily resolves basaltic volcanic edifices erupted under subaerial conditions (class A, shields) from those erupted under intraglacial conditions (class B). Jones (1969) underlined the striking contrast in slope between subaerial and subglacial volcanic landforms, and this study defines a 5° gap in average slope between the two classes, thus making slope a very diagnostic parameter. Furthermore, our results suggest that subaerial shields can be divided into two sub-classes with average slopes below 5° (subclass A1) and between 5 and 7° (subclass A2) corresponding to olivine tholeiitic and picrite shields, respectively. This a tentative result based on only 7 shields, but is in accordance with Rossi (1996) who also report that mean slopes of picrite shields (5.8°) are notably steeper than for olivine tholeiite shields (3.4°). He argued that the higher vesicularity and phenocryst content in the picrites causes higher apparent viscosity that is responsible for their steeper slopes.

The glaciovolcanic edifices can be divided into 3 groups depending on size, from small tindars (group B1) to intermediate edifices consisting of tindars, conical tuyas and complex tuyas (group B2) to large flat-topped tuyas (group B3). The plan shape indexes (ellipticity and irregularity) show a first order correlation with the classes and groups, but they are not strictly diagnostic.

Various other geomorphometric parameters were investigated in order to evaluate their potential as diagnostic parameters. The height/basal width ratio (H/W) has been widely used previously (e.g. Rossi, 1996; Smellie, 2007) and can be considered a slope estimator, but we find that the average slope based on the slope map itself is a more diagnostic geomorphometric parameter. Parameters such as summit width and crater width and depth are uncertain due to the resolution of the DEM compared to the size of the edifice summits (except for the large summit regions of group B3 flat-topped tuyas), and thus morphometric ratios such as $W_{Summit}/W_{Base}$, $W_{Crater}/W_{Base}$ (e.g. Pike, 1978; Wood, 1979; Hasenaka, 1994; Hauber et al., 2009) were not considered. However, Rossi (1996) emphasized that neither crater width nor depth is an important parameter for Icelandic shield volcano construction since these parameters are controlled by lava lake stability during the final stages of the eruption. The greatest caution when using a slope-based classification is the dependence to the DEM resolution (e.g. Evans, 2012; Grosse et al., 2012). Lower resolution DEMs will always tend to provide lower slope values due to greater averaging, and it is therefore necessary that the resolution of the DEM be within the landform process scale (e.g. Pain, 2005).

Both slope and volume are geomorphometric parameters that are fairly easy to derive and incorporate into automated mapping

**Table 4**
Comparison of size and slope parameters calculated using the concave edifice boundary (CEB) and geologic boundary (GB) delimitations for edifices of class A (subaerial shield volcanoes).

| | Concave edifice boundary delimitation (CEBD)/Geologic boundary delimitation (GBD) | | | | | | | | | | | | Percentage of parameter: CEBD/GBD | | | | | |
|---|---|---|---|---|---|---|---|---|---|---|---|---|---|---|---|---|---|---|
| | 1 | | 2 | | 3 | | 4 | | 5 | | 6 | | 1 | 2 | 3 | 4 | 5 | 6 |
| | Height (m) | | Basal area ($km^2$) | | Basal width (km) | | Height/basal width | | Volume ($km^3$) | | Mean slope (°) | | (%) | (%) | (%) | (%) | (%) | (%) |
| Burfell | 64 | 167 | 0.700 | 2.000 | 0.95 | 1.59 | 67.58 | 104.98 | 0.0110 | 0.0294 | 6.5 | 5.5 | 38 | 35 | 60 | 64 | 37 | 119 |
| Lagafell | 39 | 47 | 0.540 | 1.327 | 0.83 | 1.30 | 47.10 | 36.16 | 0.0070 | 0.0095 | 5.6 | 3.8 | 83 | 41 | 64 | 130 | 74 | 149 |
| Sandfellsdalur | 50 | 90 | 1.796 | 94.400 | 1.51 | 10.97 | 33.07 | 8.21 | 0.0200 | – | 3.3 | 1.4 | 56 | 2 | 14 | 403 | – | 235 |
| Selvogsheidi | 176 | 180 | 18.134 | 22.547 | 4.81 | 5.36 | 36.63 | 33.60 | 0.6400 | 0.7649 | 3.2 | 2.9 | 98 | 80 | 90 | 109 | 84 | 110 |
| Skalafell | 62 | 68 | 1.288 | 7.263 | 1.28 | 3.04 | 48.40 | 22.36 | 0.0190 | 0.0598 | 4.6 | 2.8 | 91 | 18 | 42 | 216 | 32 | 166 |
| Thrainskjaldarhraun | 23 | 255 | 0.953 | 102.892 | 1.10 | 11.45 | 20.87 | 22.28 | 0.0060 | – | 2.8 | 1.8 | 9 | 1 | 10 | 94 | – | 153 |
| Vatnasheidi | 56 | 119 | 1.362 | 2.723 | 1.32 | 1.86 | 42.52 | 63.91 | 0.0230 | 0.0428 | 5.3 | 4.2 | 47 | 50 | 71 | 67 | 54 | 125 |

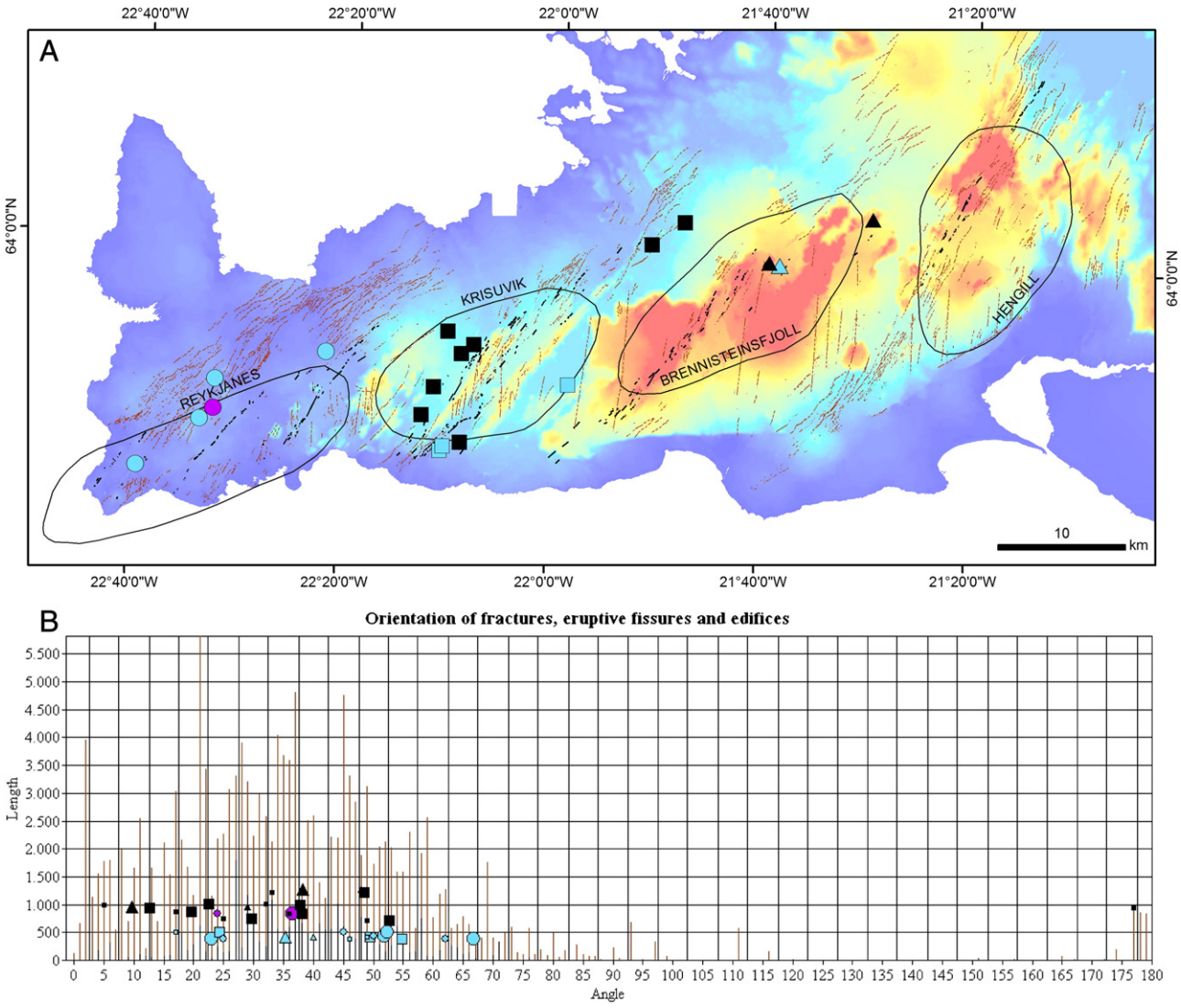


**Fig. 10.** Spatial distribution and elongation orientation of studied elongated edifices (basal E.I. >1.8) with respect to the eruptive fissures and fractures of the volcanic systems. (A) Map showing location of edifices within the volcanic systems (closed black outlines, as defined by Saemundsson, 1978) and of eruptive fissures (black lines) and faults (brown lines) mapped by Clifton and Schlische (2003) and Clifton and Kattenhorn. The edifice symbols are colored according to class and group (A2 is purple, B1 is blue and B2 is black) No edifices in class A1 or B3 have a basal E.I. >1.8. (B) Azimuth angle distribution and length of the fractures (brown) and fissures (black) mapped by Clifton and Schlische (2003), and elongation azimuths of the studied elongated edifices. Larger symbols are the basal elongation azimuth angles, while the smaller symbols are the average elongation azimuth angles of all closed elevation contours within an edifice.

procedures. At the same time, slope and volume are easy to understand from a morphological point of view, since slope is related to lithological properties and volume is a measure for eruption size. Furthermore, the variations in slope values within each edifice allows distinction of individual landform elements. Hence, the break in slope between flank and plateau at the flat-topped lava-capped tuyas (Fig. 8) coincides with the boundary between the lava cap and the hyaloclastite on the map of Saemundsson et al. (2010), and marks the boundary between intraglacial and subaerial volcanic activity. This break in slope does not delimit exactly the passage zone, since it marks the top edge of the lava cap, whereas the passage zone is located at the bottom of the lava cap, where it comes into contact with the top of the lapilli tuff/tuff breccia. However, in an orthographic view, the top edge of the lava cap may be the best approach to delineate the transition from intraglacial to subaerial volcanic activity, since it would be very difficult to detect the bottom of the near-vertical lava cap edge. The elevation difference between the lava cap edge and the passage zone will therefore depend on the thickness of the lava cap at its edge.

### 5.1. Quantitative edifice-scale morphology

In the classification scheme of Russell et al. (2014) the main subdivision of tuyas is based on edifice-scale morphology. The subdivision into four morphological classes is qualitative, except for the L/W > 2 criteria for distinction of tindars. In the following we use morphometric results to asses the morphological classification of tuyas by Russell et al. (2014).

The majority of glaciovolcanic edifices in this study are tindars (15 edifices, Table 1). All of the small group B1 edifices are tindars, as well as half of the intermediate sized group B2 edifices. They are steep-sided ridges with average slope values between 12° and 23° (Fig. 4), and maximum slope values around 30–35° (Fig. 6). They are elongated, with basal and average E.I. values >1.8, which we find is a better threshold than 2 as there is a gap of both basal and average E.I. at around 1.8. The tindars are fairly regular (I.I. values mostly below 1.10). However, some very elongated tindars are more irregular because the ridge crests often have multiple peaks, probably due to multiple eruptive vents, consisting of tuff cones in the case of Sveifluháls (Mercurio et al., 2009; Skilling

et al., 2009). We do not observe any distinct morphometric differences between pillow lava dominated tindars compared to hyaloclastite dominated tindars (Table 1). Four hyaloclastite dominated tindars have a lava cap (Table 1) of variable size (0.07–0.20 km$^2$, based on the map of Saemundsson et al., 2010). The lava caps of Geithöfdi, Blákollur and Kóngsfell can be resolved using the slope map, but they do not affect the slope histograms (Fig. 6) or the slope development as a function of height (Fig. 7).

Of the 26 analyzed glaciovolcanic edifices, Keilir (Fig. 3Q–T), which means 'cone' in Icelandic, is the only edifice that classifies as a conical tuya. This edifice is very circular, with an average E.I. of 1.34, and very regular, with an average I.I. of 1.03. It has a mean slope of 20° and maximum slopes of around 35°. It has a very small summit region, although it does have a tiny lava cap (0.02 km$^2$) that is below the resolution of the DEM.

The three edifices of group B3 can be classified as flat-topped tuyas. They have average slope values between 13.1° to 19.2° (Fig. 4), with a wide, bimodal slope distribution resulting from their steep flanks and large low-sloping summit region plateaus. They cluster in a confined field in the plan shape index diagram (Fig. 4B), being fairly regular (average I.I. 1.06–1.09) and circular, with low basal (1.31–1.44) and average E.I. values (1.35–1.67). Despite their similar morphometric characteristics, they vary lithologically. Geitafell and Geitahlid consist primarily of hyaloclastite with large lava caps, whereas Thorbjörn is a pillow dominated flat-topped tuya without a lava cap (Table 1).

Finally, we have classified 7 of the 26 edifices as complex tuyas, all in the intermediate-sized group B2. The shapes of these edifices are quite diverse, as evidenced by the spread in the plan shape index diagram (Fig. 4B), suggesting different morphological evolutions. Three types of complex tuyas can be considered. Fiskidalsfjall and Húsafell have characteristics of both tindars and flat-topped tuyas. Fiskidalsfjall has a high average E.I. of 2.56, but a low basal E.I. of 1.35. Húsafell has low E.I. values similar to flat-topped tuyas, but lacks the biomodal slope distribution and the step-wise slope trend as a function of height characteristic of the flat-topped tuyas of group B3. Hence, these two complex tuyas can be regarded as transitional edifices between tindars and flat-topped tuyas.

Driffel, Hraunssels-Vatnfell and Syllingafell (Fig. 3M–P) have relatively flat plateaus at variable heights. Driffel has a small ridge above a wider lava plateau, whereas Hraunssels-Vatnfell consists of 2 lava-capped plateaus at different elevations, and Syllingafell consists of a plateau topped by a cone. These 3 edifices are irregular, with high basal I.I. values (1.14–1.16) and intermediate to high average I.I. values (1.06–1.15). We suggest that these edifices have undergone variations in eruption style, either within the same eruption or during more than one eruptive event.

Stóra-Skogsfell and Thórdafell consist of a combination of ridges and/or cones. Stóra-Skogsfell consists of a western ridge and an eastern cone, whereas Thórdafell is composed of three variably elongated cones. The edifices have moderate average slope values (15.0°, 15.9°) and are fairly equidimensional (basal E.I. of 1.67, 1.71; average E.I. of 1.63, 2.30) and very irregular (average I.I. of 1.18, 1.28). Saemundsson et al. (2010) interpret Thórdafell as a faulted edifice dominated by a large crater suggesting that the present morphology is a result of the modification of this crater structure. Likewise, Stóra-Skogsfell is dissected by a small fissure that has modified its original shape (Saemundsson et al., 2010).

The morphometric diversity shown by the 26 glaciovolcanic edifices analyzed in this study indicates that glaciovolcanic landforms are far more complicated than the "classic" tindar and tuya division, and support the new morphological classification scheme of Russell et al. (2014). The glaciovolcanic edifices show variable lithologies that do not seem to impact their edifice-scale morphology. Tindars and flat-topped tuyas can be considered end members in a trend from small tindars to mid-sized tindars or more complex tuyas, with or without small lava caps, to large flat-topped tuyas. Mid-sized edifices (group B2) are either tindars or complex tuyas (with the exception of cone-shaped Keilir), suggesting two main types of evolutions: small tindars that continue growing as tindars maintaining their ridge shape (suggesting a fissure type source), and small tindars that evolve towards more complex shapes (suggesting a change of source, from fissure to central, and/or in source location). The fact that only one edifice is a conical tuya suggests that this type of edifice is less frequent. The group of complex tuyas is itself very diverse, showing different characteristics. Some edifices have intermediate shapes between tindars and flat-topped tuyas, whereas others seem to consist in the merging of two or more simple shapes, e.g. ridge and cone, several cones, ridge and plateau, cone and plateau, etc. These combinations suggest variations in the eruptive histories and could be considered a sign of polygenetic activity, as suggested by Russell et al. (2014). However, the observed complexities could also be the result of changes in vent geometry (linear to central or vice versa) or later modification. Finally, irregular Thórdafell is an example of a pillow mound with a large crater (Saemundsson et al., 2010) that can be considered a 'bowl-shaped tuya' dominated by the crater morphology. However, in the current classification scheme of Russell et al. (2014) there is no category for crater-dominated morphologies and hence, this type of edifice, which may have a simple eruption history, will be classified, probably inappropriately, as a complex tuya.

In terms of classification, quantification of the limits between the four tuya types proposed by Russell et al. (2014) is difficult because of the transitional nature and merging of shapes shown by several edifices. A threshold of 1.8 in E.I. values (both basal and average) can be used to distinguish tindars from the other three types. Flat-topped tuyas are distinguished by their greater overall size, their large and relatively flat summit regions, reflected in bimodal slope distributions, and their low E.I. and low to intermediate I.I. values. Taking Keilir as the only representative, conical tuyas have very low E.I. and I.I. values, very small summit regions and very steep flank slopes. The complex tuyas have variable morphometries, but are in general characterized by high I.I. values and very irregular slope distributions. However, we suggest that further analysis using a larger dataset could result in better quantitative constraints for glaciovolcanic edifices.

### 5.2. Volcanic landform evolution on Reykjanes Peninsula

It has previously been suggested that the morphology and structure of glaciovolcanic edifices are controlled by (1) tectonic regime and (2) the availability of magma at the time of the eruption (e.g. Jakobsson and Johnson, 2012). Smellie (2007) suggested that the length of edifices is strongly affected by whether the vent was linear or a point source, which supports the suggestion that the glaciovolcanic equivalents to subaerial fissures and shields are tindars and flat-topped tuyas, respectively (e.g. Andrew and Gudmundsson, 2007). Furthermore, Smellie (2007) suggested a possible evolutionary trend for mafic glaciovolcanic landforms from a pillow tindar to a tephra tindar to a mafic tuya.

Here we likewise try to asses if there are evolutionary trends among the different types of analyzed edifices. The average E.I. quantifies edifice elongation and thus can be correlated with vent type. Edifices with low E.I. are interpreted to be primarily central-vent controlled edifices; they include shields (class A), flat-topped tuyas (class B, group 3), conical tuyas (Keilir) and the complex tuyas Stóra-Skogsfell and Thórdafell from class B group 2. Edifices with high E.I. values (>1.8) are primarily fissure controlled edifices; they are the small tindars (class B, group 1) as well as the mid-sized tindars of class B group 2 (Table 1). The other 5 complex tuyas of group B2 possibly experienced a combination of central and fissure-vent geometries.

Fig. 9 summarizes the relationship between edifice volume and vent-type based on the above-mentioned ellipticity index. Larger edifices are controlled by a point-source, while smaller edifices are fissure controlled. There is a large overlap in volume where both fissure-controlled and central-vent controlled edifices occur, ranging

from approximately 0.01–0.1 km$^3$, corresponding to edifices of group B2, in agreement with the great variety of edifice shapes in this group. Hence, the tindars of group B2 are fissure controlled, whereas the conical tuya and the pillow mounds Stóra-Skogsfell and Thórdafell seem to be controlled primarily by a point-source. Tindars Krýsuvikur-Mælifell and Kóngsfell have higher basal E.I. than average E.I., which may indicate an initial fissure eruption that later localized at a point source. Other tindars in group B2 (Blákollur, Helgafell, Húsfell, Oddafell and Sandfell E) show the opposite trend, thus suggesting a continuous fissure type source. The complex tuyas Fiskidalsfjall and Húsafell have both linear and central characteristics and thus seem to be transitional edifices having been controlled by a combination of fissures and central vents The other complex tuyas of group B2 (Driffel, Hraunssels-Vatnsfell, and Syllingarfell) have more complex shapes. Their complexity may indicate variations in eruption style, different englacial lake levels during eruption, polygenetic evolution and/or post-eruptive modification.

Rossi (1996) suggested a model for the evolution of subaerial shields in Iceland, starting with a fissure eruption that concentrates into smaller vents and subsequently forms small overlapping shields. As the shield grows, the lava-delivery system will change from being centered at the cone to being extended in tubes producing large lava aprons making up to 99% of the aerial extent of the shields (Rossi, 1996). This model is similar to a glaciovolcanic landform evolution from tindars to flat-topped tuyas as suggested by Smellie (2007) and is in line with our observation of small tindars, intermediate sized transitional edifices and large flat-topped tuyas. Interestingly, Rossi (1996) suggests that the transition from small cone-centered shields to intermediate apron-producing shields occurs in a volume range (0.02 km$^3$) similar to intermediate-sized edifices analyzed here (0.018–0.050 km$^3$). Gudmundsson (1986) states that the average eruptive volume on Reykjanes Peninsula from 101 eruptive fissures is 0.11 km$^3$, while the average eruptive volume of 26 shield volcanoes is 1.11 km$^3$. However, the highest volume frequency for fissure eruptions occurs in the interval 0–0.025 km$^3$, while the highest volume frequency for shields is 0–0.25 km$^3$, suggesting that the most typical eruption scenarios show a similar volume tendency for fissure and central vent eruptions as ours and Rossi's (1996) results.

Fig. 9 also shows the volume range of edifices primarily consisting of pillow lava, hyaloclastite and hyaloclastite with a lava cap. Pillow lava dominated edifices range two orders of magnitude in volume, from the smallest analyzed tindars, to intermediate-sized tindars and complex tuyas, to Thorbjörn, the smaller of the three flat-topped tuyas. Hyaloclastite dominated edifices have nearly the same volume range as pillow lava dominated edifices. Hyloclastite edifices with a lava cap tend to be larger, but there are also small lava capped edifices like Sýrfell, Geithöfdi and Driffel. The ability to form a lava cap has been ascribed to large kilometer-size openings in the ice (Gudmundsson et al., 1997) and it is therefore surprising to observe lava caps on these very small edifices. The tindar ridge formed by the historical Gjálp eruption was 0.7–0.75 km$^3$ and did not produce any lava cap. The initial ice-thickness during the Gjálp eruption was 550–750 m and a visible subaerial phase was only a minor part of the eruption, and Gudmundsson et al. (1997) estimated that 3 km$^3$ melt water was produced during the eruption. Borehole data from Sýrfell suggest that the edifice base is at 110–140 m depth (Halldórsdóttir and Gylfadóttir, 2013), and thus its total edifice height is between 185 and 215 m and its total volume is roughly 0.03 km$^3$. If we assume that the ice melted per volume of erupted volcanic material is the same for a basaltic tindar like Sýrfell as for the basaltic-andesitic tindar produced in the Gjálp eruption, the Sýrfell eruption would have produced 0.12–0.13 km$^3$ of melt water, equivalent to a 180 m high ice cylinder with a diameter of ca. 0.9–1.0 km. This is in accordance with Gudmundsson et al. (1997), suggesting that very small lava capped edifices, such as Sýrfell, are able to penetrate a fairly thin ice sheet and create kilometer-sized openings in the ice, and consequently a lava cap.

Keilir is the only conical tuya and displays a very small lava cap. Though Keilir may have grown as a cone and produced the very small lava cap at the end of its eruption, it is also possible that it experienced post-eruptive erosion of a significant part of the lava cap. Keilir has been assigned an Early Bruhnes age by Saemundsson et al. (2010), which makes glacial erosion from Pleistocene glaciations very likely, and it is therefore possible that the only conical tuya we have analyzed is actually an erosional remnant of either a lava capped tindar or flat-topped tuya. In that case Keilir would exemplify the mentioned caveat in Russell et al.'s (2014) classification scheme, where post-eruptive processes modify the edifice so significantly that it changes its morphological category. Detailed investigation of Keilir is needed to reveal its morphological evolution. The other glaciovolcanic edifices from Early Brunhes (Geithöfdi, Driffel, Thórdafell and Thorbjörn) may also have experienced glacial erosion, but both Thórdafell and Thorbjörn display crater morphologies (Saemundsson et al., 2010), suggesting that glacial erosion was not significant on those edifices, whereas they have been faulted significantly.

### 5.3. Volcanic landform and tectonic regime

In order to evaluate the influence of the tectonic regime on the orientation of the edifices, we compared the elongation azimuths of the elongated edifices (those with basal E.I. >1.8) with the azimuths of eruptive fissure and fracture populations mapped by Clifton and Schlische (2003) and Clifton and Kattenhorn (2006) (Fig. 10). The most common fracture directions on Reykjanes Peninsula are between 041 and 060° followed by 061 and 080°, while the longest fractures strike between 021 and 040° (Clifton and Kattenhorn, 2006). Fissure swarms strike mostly 035–045° and form perpendicular to the orientation of maximum horizontal extension and occur in the axial zones of the volcanic systems (Clifton and Schlische, 2003).

Of the 19 edifices with basal E.I. >1.8, most are tindars from class B groups 1 and 2, some are complex tuyas from class B group 2, one is the conical tuya Keilir, and one is a shield (Lagafell). Most basal elongation azimuths are distributed in the interval 020–080°, coinciding with the main fracture directions (Fig. 10). The exceptions are Kóngsfell and Hraunssels-Vatnfell, which are elongated in the 00–020° interval in coincidence with N–S striking book-shelf faults also mapped by Clifton and Kattenhorn (2006). Both of these edifices are cross-cut by N–S oriented faults. A more uncertain but similar correlation is observed for less elongated edifices (Vatnsheidi and Syllingafell) with basal E.I. values between 1.5 and 1.8, which are also associated to N–S oriented faults (Table 1). Clifton et al. (2007) note that many eruptive fissures change strike for distances of up to 2 km where they intersect a zone of N–S strike-slip faults, as exemplified by the study of the Sundhnúkur fissure swarm (Jenness and Clifton, 2009). We suggest that glaciovolcanic edifices such as Kóngsfell, Hraunssels-Vatnfell and Syllingafell may also change strike influenced by N–S strike-slip faults. In general, the studied edifices do not show such a narrow clustering of orientation as the eruptive fissures (035–045°), but rather a distribution in the entire interval where there is significant fracturing and faulting. This indicates a strong tectonic control on the elongations of the edifices, independent of the proximity to the volcanic systems, and confirms the observations of Clifton and Young (2007) that individual eruptive fissures appear to have used pre-existing pathways.

Fig. 10 also shows the average elongation azimuths considering the closed elevation contours above the edifice bases. Smaller edifices show similar elongation azimuths between basal outline and average values (e.g. class B group 1), whereas some larger edifices (e.g. class B group 2) show significant differences. This observation suggests that the regional tectonic control on the shape of volcanic edifices decreases as the volcanic edifice grows.

## 6. Conclusions

The morphometric analysis of 33 basaltic volcanic edifices allows to distinguish subaerial from glaciovolcanic edifices based on average slope values. Glaciovolcanic edifices have average slopes that are at least 5° higher than subaerial shields. Slope is therefore a diagnostic parameter to distinguish between subaerial and subglacial eruption environments. A more subtle slope distinction between olivine tholeiitic and picrite shields can also be made, with olivine tholeiites having lower average slopes and picrites having higher average slopes. In addition, the variations in slope values within each edifice allows distinction of individual landform elements. Hence, for flat-topped tuyas it is possible to resolve the transition from steep flanks to flat summit regions as a clear break in slope. For lava-capped flat-topped tuyas, this break in slope coincides with the lithological boundary between lava cap and hyaloclastite mapped by Saemundsson et al. (2010), and is an estimate of the boundary between intraglacial and subaerial volcanic activity in orthographic view.

The glaciovolcanic edifices can be grouped according to volume showing a continuum of landforms ranging from small pillow tindars to large flat-topped tuyas. In general, edifice ellipticity decreases with volume suggesting that small edifices are mainly fissure controlled, whereas larger edifices are controlled by a main central vent. A group of complex tuyas of intermediate-size (0.01–0.1 $km^3$) is transitional between these two end-members, suggesting that intraglacial eruptions may start as fissure eruptions that subsequently concentrate into one main central vent.

There is a strong correlation between the elongation azimuths of the edifices and faults, suggesting a strong tectonic control on the orientation of edifices. Most edifices cluster around 020°–080°, while some edifices correlate with N–S striking book-shelf faults. This suggests that intraglacial edifices, as previously observed for subaerial fissure eruptions (Clifton and Kattenhorn, 2006; Jenness and Clifton, 2009) have used pre-existing structurally controlled pathways.

This study shows that a 20 m resolution DEM can be used for regional-scale morphometric analysis of glaciovolcanic edifices, gaining insights into the interplay of constructional and destructional processes controlling their shape. This is of particularly interest in the light of the new classification scheme of tuyas by Russell et al. (2014), which subdivide tuyas into four categories based on edifice-scale morphology. Here we present a morphometric assessment of the morphology of 26 glaciovolcanic edifices and find that 15 edifices fit the tindar category, 1 fits the conical tuya category, 3 fit the flat-topped tuya category and the remaining 7 are categorized as complex tuyas. However, further morphometric studies of glaciovolcanic edifices are encouraged in order to evaluate these categories and investigate if a quantitative morphometric classification is possible.

## Acknowledgments

The authors would like to acknowledge Kristjan Sæmundsson, Jóhann Helgasson and Amy Clifton for useful discussions as well the very useful comments from the reviewers. Furthermore, thanks are extended to the Danish Research Council and the Nordic Volcanological Center for grant support.

## References

Allen, C.C., Jercinovic, M.J., Allen, J.S.B., 1982. Subglacial volcanism in north-central British Colombia and Iceland. J. Geol. 90, 699–715.
Andrew, R.E.B., Gudmundsson, A., 2007. Distribution, structure, and formation of Holocene lava shields in Iceland. J. Volcanol. Geotherm. Res. 168 (1–4), 137–154.
Baratoux, D., Pinet, P., Toplis, M.J., Mangold, N., Greeley, R., Baptista, A.R., 2009. Shape, rheology and emplacement times of small Martian shield volcanoes. J. Volcanol. Geotherm. Res. 185 (1–2), 47–68.
Bourgeois, O., Dauteuil, O., Vliet-Lanoe, B., 1998. Pleistocene subglacial volcanism in Iceland: tectonic implications. Earth Planet. Sci. Lett. 164, 165–178.
Broz, P., Cadek, O., Hauber, E., 2013. Shape of Cinder Cones on Mars: Insight from Numerical Modelling of Ballistic Pathways. EPSC, London, England (pp. EPSC2013-240).
Caress, D.W., Clague, D.A., Paduan, J.B., Martin, J.F., Dreyer, B.M., Chadwick, W.W., Denny, A., Kelley, D.S., 2012. Repeat bathymetric surveys at 1-metre resolution of lava flows erupted at Axial Seamount in April 2011. Nat. Geosci. 5 (7), 483–488.
Clague, D.A., Paduan, J.B., Caress, D.W., Thomas, H., Chadwick Jr., W.W., Merle, S.G., 2011. Volcanic morphology of West Mata Volcano, NE Lau Basin, based on high-resolution bathymetry and depth changes. Geochem. Geophys. Geosyst. 12, QOAF03.
Clifton, A.E., Kattenhorn, S.A., 2006. Structural architecture of a highly oblique divergent plate boundary segment. Tectonophysics 419 (1–4), 27–40.
Clifton, A.E., Schlische, R.W., 2003. Fracture populations on the Reykjanes Peninsula, Iceland: comparison with experimental clay models of oblique rifting. J. Geophys. Res. Solid Earth 108 (B2), 2074.
Clifton, A.E., Young, K.D., 2007. Tectono-magmatic Segmentation on the Reykjanes Peninsula. AGU, San Francisco, USA, p. T32B-04.
Clifton, A.E., Kattenhorn, S.A., Young, K.D., Jenness, M., 2007. Control of Eruptive Fissure Geometries by the Preexisting Structural Fabric at an Oblique Spreading Center, SW Iceland. EGU, Vienna, Austria, p. 08730.
Davidson, J., De Silva, S., 2000. Composite volcanoes. In: Sigurdsson, H., Houghton, B., McNutt, R.L., Rymer, H., Stix, J. (Eds.), Encyclopedia of Volcanoes. Academic Press, San Diego, California, USA, pp. 663–681.
Einarsson, P., Saemundsson, K., 1987. Earthquake epicenters 1982–1985 and volcanic systems in Iceland. In: Sigfússon, T. (Ed.), Íhlutarins edli: Festschrift for Porbjörn Sigurgeirsson. Menningarsjódur, Reykjavík.
Euillades, L.D., Grosse, P., Euillades, P.A., 2013. NETVOLC: an algorithm for automatic delimitation of volcano edifice boundaries using DEMs. Comput. Geosci. 56, 151–160.
Evans, I.S., 2012. Geomorphometry and landform mapping: what is a landform? Geomorphology 137 (1), 94–106.
Favalli, M., Tarquini, S., Fornaciai, A., Boschi, E., 2009. A new approach to risk assessment of lava flow at Mount Etna. Geology 37 (12), 1111–1114.
Fornaciai, A., Favalli, M., Karátson, D., Tarquini, S., Boschi, E., 2012. Morphometry of scoria cones, and their relation to geodynamic setting: a DEM-based analysis. J. Volcanol. Geotherm. Res. 217–218, 56–72.
Francis, P.W., Oppenheimer, C., 2004. Volcanoes. Oxford University Press.
Garvin, J.B., 1996. Topographic characterization and monitoring of volcanoes via airborne laser altimetry. In: McGuire, W.J., Jones, A.P., Neuberg, J. (Eds.), Volcano Instability on the Earth and Other Planets. Geological Society Special Publication, pp. 137–152.
Grosse, P., van Wyk de Vries, B., Petrinovic, I.A., Euillades, P.A., Alvarado, G.E., 2009. Morphometry and evolution of arc volcanoes. Geology 37 (7), 651–654.
Grosse, P., van Wyk de Vries, B., Euillades, P.A., Kervyn, M., Petrinovic, I.A., 2012. Systematic morphometric characterization of volcanic edifices using digital elevation models. Geomorphology 136 (1), 114–131.
Grosse, P., van Wyk de Vries, B., Euillades, P.A., Euillades, L.D., 2014. A global database of composite volcano morphometry. Bull. Volcanol. 76, 784.
Gudmundsson, A., 1986. Mechanical aspects of postglacial volcanism and tectonics of the Reykjanes Peninsula, southwest Iceland. J. Geophys. Res. Solid Earth 91 (B12), 12711–12721.
Gudmundsson, A., 1995. Infrastructure and mechanics of volcanic systems in Iceland. J. Volcanol. Geotherm. Res. 64 (1–2), 1–22.
Gudmundsson, M.T., Sigmundsson, F., Björnsson, H., 1997. Ice-volcano interaction of the 1996 Gjálp subglacial eruption, Vatnajökull, Iceland. Nature 389, 954–957.
Halldórsdóttir, S., Gylfadóttir, S.S., 2013. Svartsengi — Reykjanes. Hita- og Thrýstingsmælingar. Technical Report from Isor, Ísor-2013/021 (in Icelandic).
Hasenaka, T., 1994. Size, distribution, and magma output rate for shield volcanoes of the Michoacán-Guanajuato volcanic field, Central Mexico. J. Volcanol. Geotherm. Res. 63 (1–2), 13–31.
Hauber, E., Bleacher, J., Gwinner, K., Williams, D., Greeley, R., 2009. The topography and morphology of low shields and associated landforms of plains volcanism in the Tharsis region of Mars. J. Volcanol. Geotherm. Res. 185 (1–2), 69–95.
Hickson, C.J., 2000. Physical controls and resulting morphological forms of quaternary ice-contact volcanoes in western Canada. Geomorphology 32, 239–261.
Hiatt, A.R., Pollock, M., Edwards, B.R., Hauksdottir, S., Williams, M., Reinthal, M., 2013. Estimated hydrostatic/cryostatic pressure during emplacement of pillow lavas at Undirhlithar quarry, Reykjanes Peninsula, southwest Iceland. AGU; San Francisco, USA, V41D-2840.
Inbar, M., Gilichinsky, M., Melekestsev, I., Melnikov, D., Zaretskaya, N., 2011. Morphometric and morphological development of Holocene cinder cones: a field and remote sensing study in the Tolbachik volcanic field, Kamchatka. J. Volcanol. Geotherm. Res. 201 (1–4), 301–311.
Jakobsson, S.P., Gudmundsson, M.T., 2008. Subglacial and intraglacial volcanic formations in Iceland. Jökull 58, 179–196.
Jakobsson, S.P., Johnson, G.L., 2012. Intraglacial volcanism in the Western Volcanic Zone, Iceland. Bull. Volcanol. 74 (5), 1141–1160.
Jakobsson, S.P., Jónsson, J., Shido, F., 1978. Petrology of the western Reykjanes peninsula, Iceland. J. Petrol. 19 (4), 669–705.
Jenness, M., Clifton, A., 2009. Controls on the geometry of a Holocene crater row: a field study from southwest Iceland. Bull. Volcanol. 71 (7), 715–728.
Jóhannesson, H., 1980. Jarðlagaskipan og þróun rekbelta á Vesturlandi [Evolution of the rift zones in western Iceland]. Náttúrufræðingurinn 50, 13–31.
Jones, J.G., 1969. Intraglacial volcanoes of the Laugarvatn region, south west Iceland 1. Q. J. Geol. Soc. 124, 197–211.
Jones, J.G., Nelson, P.H.H., 1970. The flow of basalt from air into water — its structural expression and stratigraphic significance. Geol. Mag. 107 (1), 13–19.
Karátson, D., Favalli, M., Tarquini, S., Fornaciai, A., Wörner, G., 2010. The regular shape of stratovolcanoes: a DEM-based morphometrical approach. J. Volcanol. Geotherm. Res. 193 (3–4), 171–181.

Kervyn, M., Kervyn, F., Goossens, R., Rowland, S.K., Ernst, G.G.J., 2007. Mapping volcanic terrain using high-resolution and 3D satellite remote sensing. Geol. Soc. Lond., Spec. Publ. 283 (1), 5–30.
Kervyn, M., Ernst, G.G.J., Carracedo, J., Jacobs, P., 2012. Geomorphometric variability of "monogenetic" volcanic cones: evidence from Mauna Kea, Lanzarote and experimental cones. Geomorphology 136 (1), 59–75.
Kjartansson, G., 1960. Geological map of Iceland. 1:250.000. Reykjavik, Iceland Survey Department.
Kjartansson, G., 1966. A comparison of table mountains in Iceland and the volcanic Island of Surtsey off the south coast of Iceland (english summary). Natturufroeingurinn 36, 1–34.
Komatsu, G., Arzhannikov, S.G., Arzhannikova, A.V., Ershov, K., 2007. Geomorphology of subglacial volcanoes in the Azas Plateau, the Tuva Republic, Russia. Geomorphology 88, 312–328.
Kortz, B.E., Head III, J.W., 2001. Comparisons of Volcanic Fields on Venus, Earth and Mars. LPSC, Houston, USA, p. 1422.
Levi, S., Audunsson, H., Duncan, R.A., Kristjansson, L., Gillot, P., Jakobsson, S.P., 1990. Late Pleistocene geomagnetic excursion in Icelandic lavas: confirmation of the Laschamp excursion. Earth Planet. Sci. Lett. 96 (3–4), 443–457.
Matthews, W.H., 1947. "Tuyas", flat-topped volcanoes in northern British Colombia. Am. J. Sci. 245, 560–570.
McKnight, S.B., Williams, S.N., 1997. Old cinder cone or young composite volcano?: The nature of Cerro Negro, Nicaragua. Geology 25 (4), 339–342.
Mercurio, E.C., Skilling, I.P., Cameron, B., 2009. Construction and evolution of an ice-confined basaltic eruptive fissure complex: Sveifluhals, SW Iceland. AGU; San Francisco, USA, V23D-08.
Michon, L., Saint-Ange, F., 2008. Morphology of Piton de la Fournaise basaltic shield volcano (La Réunion Island): characterization and implication in the volcano evolution. J. Geophys. Res. (B3), B03203.
Moore, J.G., Mark, R.K., 1992. Morphology of the Island of Hawaii. GSA Today 2 (12).
Mouginis-Mark, P.J., Rowland, S.K., Garbeil, H., 1996. Slopes of Western Galapagos volcanoes from airborne interferometric radar. Geophys. Res. Lett. 23 (25), 3767.
Noe-Nygaard, A., 1940. Sub-glacial volcanic activity in ancient and recent times (Studies in the palagonite-system of Iceland no. 1). Tom. 1, no. 2. Folia Geogr. Dan. 1, 1–67.
Pain, C.F., 2005. Size does matter: relationships between image pixel size and landscape process scales. In: Zerger, A., Argent, R.M. (Eds.), MODSIM 2005 International Congress on Modelling and Simulation Modelling and Simulation Society of Australia and New Zealand, pp. 1430–1436.
Pike, R.J., 1978. Volcanoes on the inner planets: some preliminary comparisons of gross topography. Proc. Lunar Planet. Sci. Conf. 9th, 3239–3273.
Pike, R.J., Evans, I.S., Hengl, T., 2009. Geomorphometry: a brief guide. Anonymous Developments in soil Science. Elsevier B. V, pp. 3–30.
Plescia, J.B., 2004. Morphometric properties of Martian volcanoes. J. Geophys. Res. 109, E03003. http://dx.doi.org/10.1029/2002JE002031.
Pollock, M., Edwards, B.R., Bowman, L., Was, E., Alcorn, E., Hauksdottir, S., 2013. Dynamics of pillow-dominated subglacial eruptions recorded in Undirhlithar quarry, Reykjanes Peninsula, southwest Iceland. IAVCEI Scientific Assembly, Kagoshima, Japan.
Porter, S.C., 1972. Distribution, morphology, and size frequency of cinder cones on Mauna Kea Volcano, Hawaii. Geol. Soc. Am. Bull. 83 (12), 3607–3612.
Robinson, J.E., Eakins, B.W., 2006. Calculated volumes of individual shield volcanoes at the young end of the Hawaiian Ridge. J. Volcanol. Geotherm. Res. 151 (1–3), 309–317.
Romstad, B., Etzelmuller, B., 2009. Structuring the digital elevation model into land form elements through watershed segmentation of curvature. Proceedings of Geomorphometry. University of Zurich, Zurich, pp. 55–60.
Rossi, M.J., 1996. Morphology and mechanism of eruption of postglacial shields in Iceland. Bull. Volcanol. 57, 530–540.
Rowland, S.K., 1996. Slopes, lava flow volumes, and vent distributions on Volcán Fernandina, Galápagos Islands. J. Geophys. Res. 101 (B12), 27657.
Rowland, S.K., Garbeil, H., 2000. Slopes of oceanic basalt volcanoes. Geophys. Monogr. 116, 223.
Russell, J.K., Edwards, B.R., Porritt, L., Ryane, C., 2014. Tuyas: A Descriptive Genetic Classification. Quat. Sci. Rev. 87, 70–81.
Saemundsson, K., 1978. Fissure swarms and central volcanoes of the neovolcanic zones of Iceland. Geol. J. Spec. Issue 10, 415–432.
Saemundsson, K., Jóhannesson, H., Hjartarson, Á., Kristinsson, S.G., Sigurgeirsson, M.Á., 2010. Geological map of Southewest Iceland. Iceland Geosurvey. 1:100000.
Schenk, P.M., Wilson, R.R., Davies, A.G., 2004. Shield volcano topography and the rheology of lava flows on Io. Icarus 169 (1), 98–110.
Schopka, H.H., Gudmundsson, M.T., Tuffen, H., 2006. The formation of Helgafell, southwest Iceland, a monogenetic hyaloclastite ridge: Sedimentology, hydrology and volcano-ice interaction. J. Volcanol. Geotherm. Res. 152, 359–377.
Schilling, S.P., 1998. LAHARZ; GIS programs for automated mapping of lahar-inundation hazard zones. USGS Open-File Report, pp. 98–638.
Skilling, I.P., Mercurio, E., Cameron, B.I., 2009. Ice-confined basaltic eruptive fissure complexes in Iceland: Accessible analogs for understanding shallow submarine ridge construction. AGU, San Francisco, USA.
Sigmundsson, F., 2006. Iceland Geodynamics. Crustal Deformation and Divergent Plate Tectonics. Springer, Germany.
Smellie, J.L., 2000. Subglacial eruptions. In: Sigurdsson, H. (Ed.), Encyclopaedia of Volcanoes. Academic Press, San Diego, pp. 403–418.
Smellie, J.L., 2007. Quaternary volcanism: subglacial landforms. In: Elias, S.A. (Ed.), Encyclopedia of Quaternary Sciences. Elsevier, Amsterdam, pp. 784–798.
Smellie, J.L., Johnson, J.S., McIntosh, W.C., Esser, R., Gudmundsson, M.T., van Hambrey, M.J., van Wyk de Vries, B., 2008. Six million years of glacial history recorded in volcanic lithofacies of the James Ross Island Volcanic Group. Antarctic Peninsula, Palaeogeography, Palaeoclimatology, Palaeoecology 260, 122–148.
Smith, D.K., 1996. Comparison of the shapes and sizes of seafloor volcanoes on Earth and "pancake" domes on Venus. J. Volcanol. Geotherm. Res. 73 (1–2), 47–64.
Strech, R.C., Mitchell, N.C., Portaro, R.A., 2006. A morphometric analysis of the submarine volcanic ridge south-east of Pico Island, Azores. J. Volcanol. Geotherm. Res. 156, 35.
Székely, B., Karátson, D., 2004. DEM-based morphometry as a tool for reconstructing primary volcanic landforms: examples from the Börzsöny Mountains, Hungary. Geomorphology 63 (1–2), 25–37.
Van Asselen, S., Seijmonsbergen, A.C., 2006. Expert-driven semi-automated geomorphological mapping for a mountainous area using a laser DTM. Geomorphology 78 (3–4), 309–320.
Van Bemmelen, R.W., Rutten, M.G., 1955. Table mountains of Northern Iceland. E.J. Brill, Leiden, Netherlands.
Walker, G.P.L., 1965. Some aspects of Quaternary volcanism in Iceland. Transactions of The Leicester Literary and Philosophial SocietyLIX, pp. 25–40.
Walker, G.P.L., 1993. Basaltic-volcano systems. Geol. Soc. Lond. Spec. Publ. 76, 3–38.
Was, E., Edwards, B.R., Pollock, M., Hauksdottir, S., Gudmundsson, M.T., Hiatt, A.R., Perpalaj, A., Plascencia, E., Reinthall, M., Silverstein, A., 2013. Along-axis variation in volcanology and geochemistry of a pillow-dominated tindar: Comparison of exposures in Undirhlithar and Vatnskarth quarries, Reykjanes Peninsula, Iceland. AGU, San Francisco, USA.
Wood, C.A., 1979. Monogenetic Volcanoes of the Terrestrial Planets. LPSC, Houston, USA, pp. 2815–2840.
Wood, C.A., 1980a. Morphometric evolution of cinder cones. J. Volcanol. Geotherm. Res. 7, 387–413.
Wood, C.A., 1980b. Morphometric analysis of cinder cone degradation. J. Volcanol. Geotherm. Res. 8, 137–160.
Wormald, S.C., Wright, I.C., Bull, J.M., Lamarche, G., Sanderson, D.J., 2012. Morphometric analysis of the submarine arc volcano Monowai (Tofua–Kermadec Arc) to decipher tectono-magmatic interactions. J. Volcanol. Geotherm. Res. 239–240, 69–82.